Acta Geologica Sinica (English Edition), 2019, 93(5): 1559–1579

Detrital Zircon U-Pb Dating of Nanshuangyashan Formation in the Jiamusi Massif, NE China and its Tectonic Implications

CUI Weilong[1, 2], ZENG Zhen[3, 4, *], ZHANG Xingzhou[3], LIU Zhenghong[3], WANG Shijie[3], PU Jianbin[3], FU Qiulin[3] and GUO Ye[3]

[1] *State Key Laboratory of Lithospheric Evolution, Institute of Geology and Geophysics, Chinese Academy of Sciences, Beijing 100029, China*
[2] *College of Earth and Planetary Sciences, University of Chinese Academy of Sciences, Beijing 100049, China*
[3] *College of Earth Sciences, Jilin University, Changchun 130061, China*
[4] *China Aerospace Academy of Architectural Design and Research Co., Ltd, Beijing 100162, China*

Abstract: A suite of the fossil-rich marine-land interbedded strata (Nanshuangyashan Formation) is distributed at the eastern margin of the Jiamusi massif in the eastern Heilongjiang Province, NE China. The authors had recently discovered a suite of arkose beneath the marine-land interbedded strata, which overlays unconformably on the Permain granite in the eastern margin of the Jiamusi massif. The LA-ICP-MS zircon U-Pb dating indicate that all detrital zircons from the analysed four arkose samples show the four population ages of ＞800 Ma, 538–481 Ma, 269–250 Ma and 223–215 Ma. The former three population ages are widely recorded in the Jiamusi-Khanka massif and the Songnen massif. The later group is the minimal age population in the analyzed samples, limiting the sedimentation time of the arkoses occurred after the Late Triassic. At present, the minimal age population is not recorded in the Jiamusi massif, but the granites with the ages of 228–210 Ma are widely distributed in the Songnen-Zhangguangcai Range massif and the Khanka massif. The predominantly Permian zircons are characterized by oscillatory zoning and euhedral shapes, with variable zircon $\varepsilon_{\rm Hf}(t)$ values (−5.5 to +11.2), indicating that they were derived from mixture sources, possibly mixed with components of the Songnen-Zhangguangcai Range massif and the Jiamusi-Khanka massif. These results, combined with regional analyses, indicate that the closing of Mudanjiang ocean and Panthalassa ocean possibly existed from Early Permian to Late Triassic.

Key words: Jiamusi massif, Nanshuangyashan Formation, Late Triassic, detrital zircon, NE China

Citation: Cui et al., 2019. Detrital Zircon U-Pb Dating of Nanshuangyashan Formation in the Jiamusi Massif, NE China and its Tectonic Implications. Acta Geologica Sinica (English Edition), 93(5): 1559–1579. DOI: 10.1111/1755-6724.14351

1 Introduction

The Jiamusi massif, characterized by widely exposed amphibolite-granulite facies metamorphosed supercrust rocks (khondalite), is in the eastern part of the NE China (Zhang et al., 2015). The massif is tectonically located in the easternmost part of the Central Asian Orogenic Belt held by the two ancient plates of North China and Siberia, and in the eastern part of the Mesozoic accretionary complex belt on the continental margin of the Western Pacific Ocean (Fig. 1), so that the junction area is of great significance to understand the tectonic transformation of the Paleo-Asian to the Pacific tectonic regimes. The previous studies generally believed that the Jiamusi massif is a Precambrian massif involved into the eastern Asian Variscan geosyncline fold system (Huang et al., 1977), or the Paleozoic accretional orogenic belt neighboring the craton (Sengör et al., 1996; Li et al., 1998; Dobretsov et al., 2005). However, a growing evidence shows that NE China (the Jiamusi, Songnen and Erguna-Xing'an massifs) and neighboring Russia (Bureya and Khanka massifs) are considered to be an integrated microcontinent in the Early Paleozoic (Khanchuk et al., 2001; Buslov et al., 2004; Zhang et al., 2012, 2015). The integrated microcontinent is mainly composed of 5 microplates (the Jiamusi, Songnen, Erguna-Xing'an, Bureya and Khanka massifs) with the Precambrian basement (Wilde et al., 2000, 2003; Ge et al., 2005; Karsakov et al., 2008; Zhou et al., 2010, 2011a, 2011b; Zhang et al., 2012), on which the unmetamorphosed Paleozoic sedimentary covers were developed after the Salair orogeny (Wang et al., 2008; Zhou et al., 2009a; Zhang et al., 2008, 2011). In terms of the integrated unit, Chinese scholars name it the Heilongjiang Plate or the Jiamusi-Mongolia Block (Zhang et al., 2015; Wang et al., 2008), and Russian scholars call it the Amur Microcontinent or Superterrane (Buslov et al., 2004; Bussien et al., 2011; Sorokin et al., 2014).

A set of Permian granites, with zircon ages between 294–258 Ma (Wu et al., 2001, 2002; Huang et al., 2008; Yu et al., 2013a; Bi et al., 2014, 2015, 2016; Pu et al., 2015), and volcanic rocks, with zircon ages between 293–263 Ma (Meng et al., 2008; Bi et al., 2017), have been discovered successively in the Jiamusi massif, especially in the eastern part of the massif, in the last 2 decades (Fig. 2). These granites and volcanic rocks are identified as magmatic arc origin on active continental margin by

* Corresponding author. E-mail: 23911989@qq.com

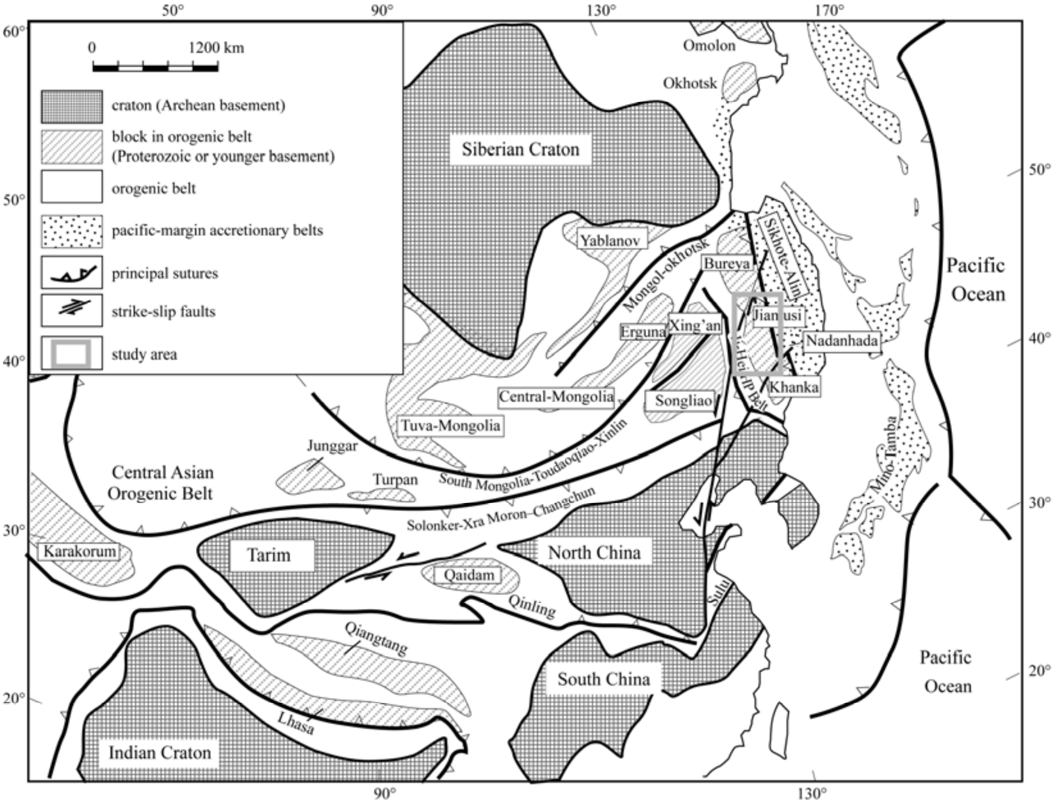

Fig. 1. Schematic tectonic map showing the main subdivisions of central and eastern Asia and location of the study area (Zhou et al., 2009b, 2014).

geochemical characteristics (Huang et al., 2008; Yu et al., 2013a; Bi et al., 2014, 2015, 2016, 2017). It shows that Jiamusi massif, as the eastern continental margin of Heilongjiang Plate, underwent the evolution of active continental margin related to subduction during Permian. However, the relationship between the tectonic properties of the eastern continental margin of the Jiamusi massif and the early Mesozoic tectonic evolution has been lacking direct evidence.

The Nanshuangyashan Formation in the Hulin, Yingchun and Mishan regions is made of a suite of coarse sandstone, feldspar sandstone, fine sandstone, Tuff siltstone, silty mudstone and mudstone, containing the Norian bivalve fauna (Zhou et al., 1962; HBGMR, 1993; Zhang et al., 2015). However, no precise depositional ages based on isotopic geochronological data have been reported. In this paper, we investigated the Late Triassic strata (Nanshuangyashan Formation) of Fangshan and Yingchun area at the eastern margin of the Jiamusi massif. And in Fangshan area we measured a section, it is found that the middle part of the strata is mainly composed of siltstones and mudstones, which are rich in fossils, while the lower part is coarse sandstones and feldspar sandstones without fossil. In a 20-meter long exploratory trench, we recognized nearly 1.5-meters thick granitic conglomerate, which is unconformity on the Permian granite (Figs. 3, 4a, 4b). The occurrence of unconformity is 329°∠39°. That provides direct geological evidence for the study of the tectonic relationship between the Permian granite and Early Mesozoic strata in the eastern margin of the Jiamusi massif. Based on this, the detrital zircon geochronology of feldspar sandstones with no fossils in the lower part of the stratum is emphatically analyzed in order to further determine the age relationship between the feldspar sandstones and the upper Late Triassic fossil-bearing strata and the characteristics of their sedimentary source areas, and to distinguish the early Mesozoic tectonic properties and their evolution in the eastern margin of the Jiamusi massif.

2 Geological Background

2.1 Geological setting

The Jiamusi massif is a major tectonic unit in the eastern part of NE China. It is bounded by Mudanjiang fault in the west and adjacent to Zhangguangcai Range in the east margin of the Songnen block, Tongjiang-Mishan fault in the East and connected with Nadanhada Mesozoic accretionary complex (or Wandashan Orogeny), Dunmi fault in the South (Fig. 2). The massif is characterized by widely exposed Amphibolite-granulite facies metamorphosed supercrust rocks (520–480 Ma) and associated contemporaneous granite (Wilde et al., 2000, 2003; Wu et al., 2001, 2000, 2003; Wen et al., 2008). Its tectonic and sedimentary evolution records of the late Paleozoic period are well preserved in the eastern margin of the block, and neritic facie of the Devonian and marine-continental interfacies of the early Carboniferous are unconformity on the metamorphic crystalline basement (HBGMR, 1993; Fu et al., 2016), the Visean, Serpukhoviav, Bashkirian and

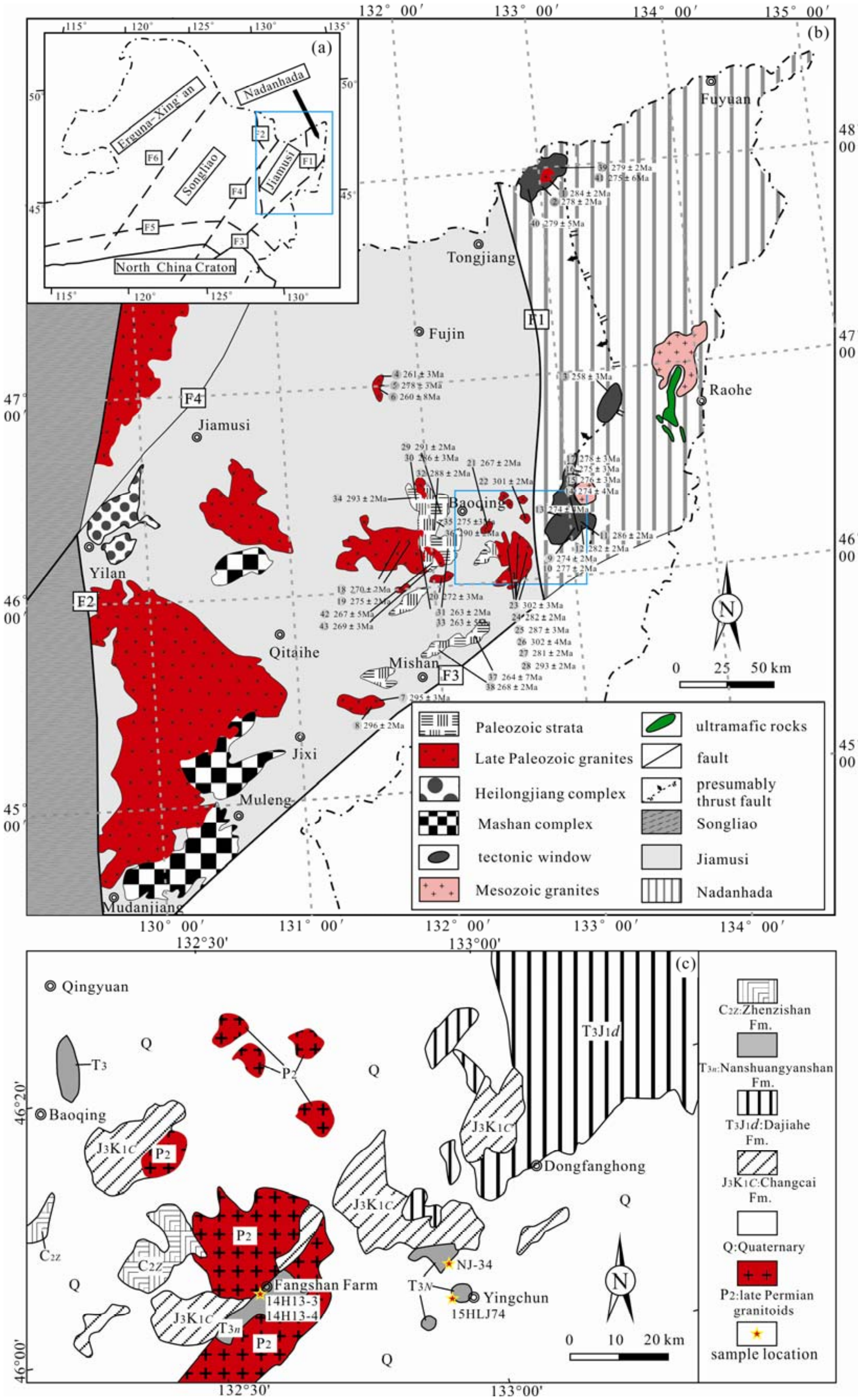

Fig. 2. A simplified geological sketch map of NE China and adjacent areas (after Zhang et al.,2006 and HBGMR, 1987).
F1-Xihot-Alin fault; F2-Mudangjiang fault;F3-Dunhua-Mishan stripe fault belt; F4-Yitong-Yilan stripe-slip fault; F5-Xar Moron River suture belt; F6-Nenjiang-Balihan stripe-slip fault (the age data were cited from Yu et al., 2013a; Bi et al., 2014, 2015, 2016, 2017; Yang et al., 2015; Sun et al., 2015; Meng et al., 2008 and unpublished data, seen Table 1).

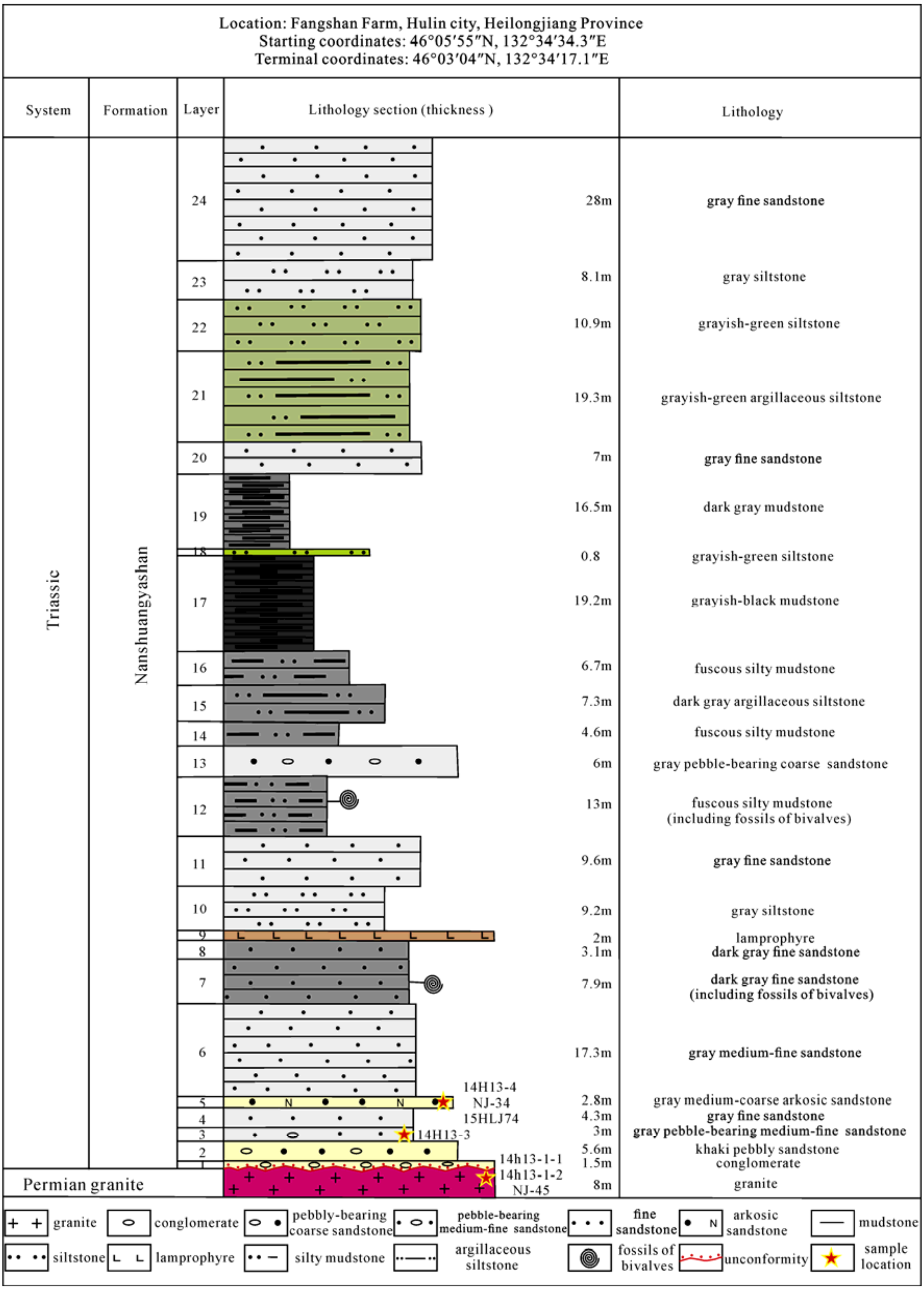

Fig. 3. Field section histogram of samples in Nanshuangyashan and sampling location (14h13-1-1 and 14h13-1-2 were cited from Pu et al., 2015).

Moscovian stage deposits are absent, and continental sediments with Angaran flora are characterized by their initial development. The latter two are the common characteristics of the whole NE China, reflecting the uplift tectonic background of the NE China in the middle Carboniferous. Starting from the Late Carboniferous, the

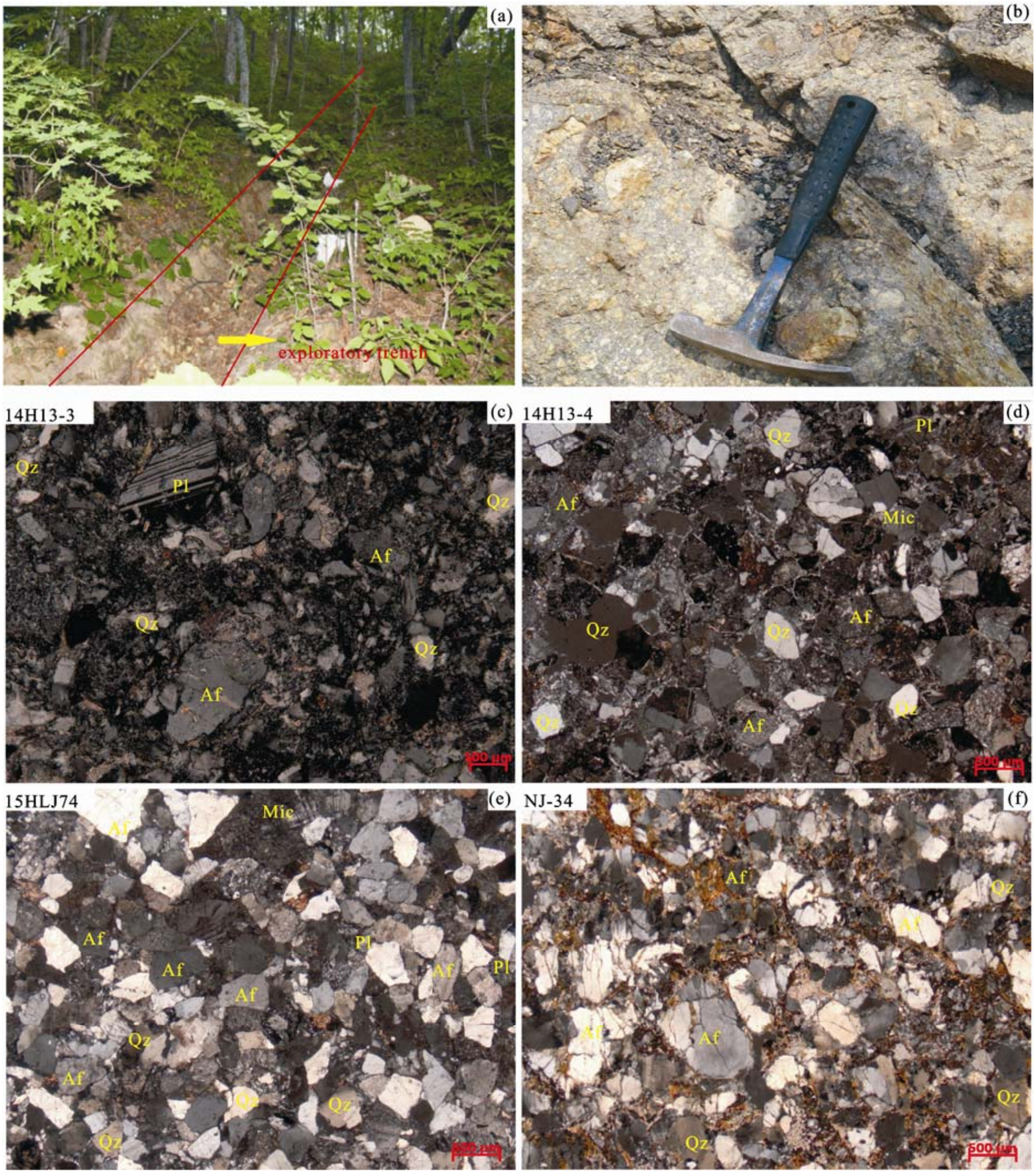

Fig. 4. Representative field photographs and micrographs of samples in Nanshuangyashan Formation.
(a) the unconformity, between Permian granite and Nanshuangyashan Formation, was recognized in field exploratory trench; (b) basal conglomerate of the Nanshuangyashan Formation; (c), (d), (e) and (f) are micrographs of 14H13-3, 14H13-4, 15HLJ74 and NJ-34 in the Nanshuangyashan Formation respectively.

sedimentary setting in the whole NE China was changed greatly and a suite of the terrestrial facies sedimentary-volcanic formation marked by abundant Angara flora was formed (Huang, 1982; HBGMR, 1993). The Lower-Middle Permian is mainly composed of the terrestrial volcanic rocks with interbedded sedimentary rocks, in which the zircon ages of the volcanic rocks are 293 to 263 Ma (Meng et al., 2008). And the Upper Permian consists dominantly of coarse clastic sedimentary rocks, containing abundant plant remains, and tuff. The Triassic strata are generally absent from broad areas of the NE China, only the Upper Triassic strata (Nanshuangyashan Formation) are exposed in the Mishan area in the southeast of the Jiamusi massif (Fig. 5).

In recent 20 years, it has been found that previous confirmed Proterozoic granites in the Jiamusi massif (HBGMR, 1993) was partly formed in Permian with zircon ages ranging from 270 Ma to 254 Ma (Wu et al.,

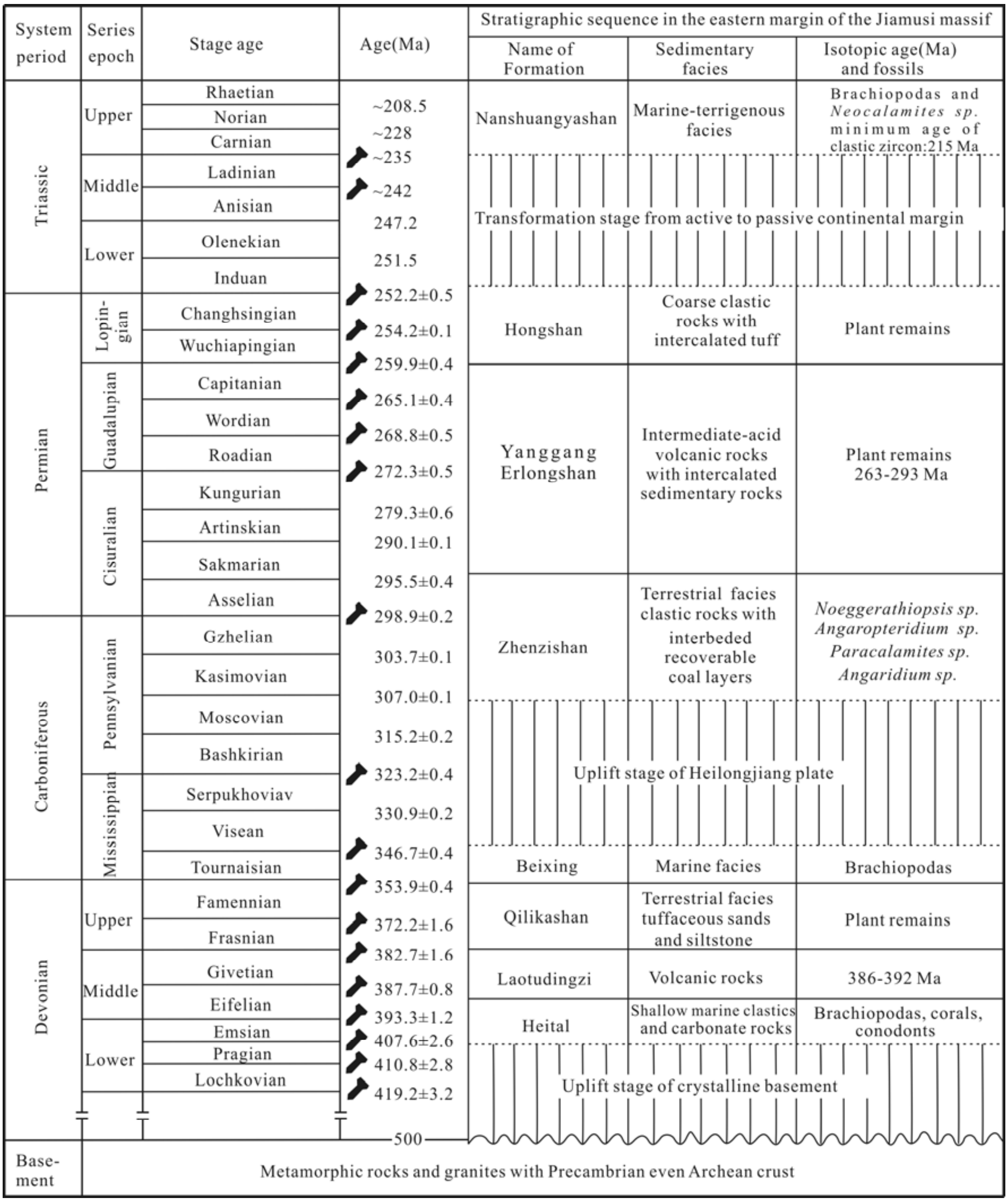

Fig. 5. Stratigraphic sequence in the eastern margin of the Jiamusi massif (Zhang et al., 2015).

2001), especially a set of Permian intermediate-acid volcanic rocks, with zircon ages ranging from 293 Ma to 263 Ma, were found in the eastern margin of the Jiamusi massif (Meng et al., 2008; Xu et al., 2012; Bi et al., 2017). These granites and volcanic rocks generally show geochemical characteristics of active continental margin (Meng et al., 2008; Huang et al., 2008; Xu et al., 2012; Yu et al., 2013a; Bi et al., 2014, 2015, 2016, 2017), indicating that the eastern part of Jiamusi massif was in the active continental margin tectonic background, related to plate subduction during the Permian. A set of Late Triassic marine-continental interfacies strata has been developed between the Late Paleozoic stratas in the eastern margin of the Jiamusi massif and the Mesozoic accretionary complex in the western Nadanhada accretionary complex. Zhou (1962) firstly name it Nanshuangyashan Formation, mainly composed of a set of coarse sandstone, feldspar sandstone, fine sandstone, siltstone and mudstone. The middle-lower part is rich in marine fossils and the upper part contains plant fossils (Zhou et al., 1962; Kang et al., 1979; Qu et al., 1997). As no direct contact relationship, between the marine-continental interfacies strata and two units (the Jiamusi massif and the Nadanhada accretionary complex), has been found in the past, there have been different understandings about its genetic environment and tectonic significance for a long time. Based on the unconformity between newly discovered sandstone and Permian granite, and the age analysis of sandstone, a new understanding of the tectonic significance of this set of strata is proposed in this paper.

2.2 Sample description

Four rock samples were collected from the Nanshuangyashan Formation in Fangshan Farm and Yingchun (Fig. 2c). The Nanshuangyashan Formation are mainly composed of conglomerate, arkosic sandstone, silty mudstone, mudstone, siltstone and argillaceous siltstone in the research area. Also, some strata contain fossils of bivalves. The rock types are all feldspar sandstones with no fossils in the lower part of the section. Most of these feldspar sandstones are of medium-coarse grained clastic texture, and the clastic content is more than 85%. They are mainly composed of feldspar (30–45%), quartz (50–60%) and a small amount of debris (< 5%). The maturity of debris particles is low, most of them are angular-subangular, poor sorting and calcareous cementation (Figs. 4c–f). Samples 14H13-3 and 14H13-4 were collected from Fangshan Farm (46°03′01″N, 132°34′11″E). Under sample 14H13-3, a set of granitic conglomerates was unconformity on the Permian granite. Sample 14H13-4 layers were offset and quartz debris increased. Sample 15HLJ74 was taken from the west of Yingchun (46°06′47″N, 132°53′41″E), and sample NJ-34 was taken from the north of Yingchun (46°08′31″N, 132°50′41″E).

3 Analytical Methods

3.1 Zircon U-Pb dating

The zircon U-Pb dating and trace element analyses of samples (14H13-3, 14H13-4, 15HLJ74, NJ-34) were carried out at the Key Laboratory of Mineral Resources Evaluation in Northeast Asia, Ministry of Land and Resources, Jilin University, Changchun, China. Helium was used as carrier gas to provide efficient aerosol transport to the ICP and minimize aerosol deposition around the ablation site and within the transport tube (Eggins et al., 1998; Jackson et al., 2004). Argon was used as the make-up gas and was mixed with the carrier gas via a T–connector before entering the ICP. The analysis spots

Table 1 Radiometric ages of the Permian magmatic events along the eastern part of the Jiamusi Massif

No.	Locality	Lithology	Formation	Dating method	Age (Ma)	Reference
1	Liulian	Granodiorite	*	LA-ICP-MS zircon U-Pb	284±2	Yu et al., 2013
2		hornblende-gabbro	*	LA-ICP-MS zircon U-Pb	278±2	Yu et al., 2013
3	Shichang	Basaltic gravel	*	LA-ICP-MS zircon U-Pb	258±3	Unpublished data
4	Jinshan	Monzogranite	*	LA-ICP-MS zircon U-Pb	261±3	Bi et al., 2014
5		Monzogranite	*	LA-ICP-MS zircon U-Pb	278±3	Bi et al., 2014
6		Granodiorite	*	LA-ICP-MS zircon U-Pb	260±8	Bi et al., 2014
7	Huangfengshan	Monzogranite	*	LA-ICP-MS zircon U-Pb	295±3	Yang et al., 2014
8	Tiexi	Diorite	*	LA-ICP-MS zircon U-Pb	296±2	Yang et al., 2014
9	Shuguang	Gabbro	*	LA-ICP-MS zircon U-Pb	274±2	Bi et al., 2015
10		Plagiogranite	*	LA-ICP-MS zircon U-Pb	277±2	Bi et al., 2015
11	Rizhao	Hornblende gabbro	*	LA-ICP-MS zircon U-Pb	286±2	Bi et al., 2015
12		Hornblende gabbro	*	LA-ICP-MS zircon U-Pb	282±2	Bi et al., 2015
13	Hamatong	Metabasalt	*	LA-ICP-MS zircon U-Pb	274±4	Unpublished data
14	Dongfanghong	Hornblende gabbro	*	SHRIMP zircon U-Pb	274±4	Sun et al., 2015
15		Hornblende gabbro	*	SHRIMP zircon U-Pb	276±3	Sun et al., 2015
16		Metabasalt	*	LA-ICP-MS zircon U-Pb	275±3	Unpublished data
17		Gabbro	*	LA-ICP-MS zircon U-Pb	278±3	Zeng et al., 2017
18	Liudao	Graphic granite	*	LA-ICP-MS zircon U-Pb	270±2	Bi et al., 2016
19	Longtouqiao	Gabbro-diorite	*	LA-ICP-MS zircon U-Pb	275±2	Bi et al., 2016
20	Liumao	Alkali feldspar granite	*	LA-ICP-MS zircon U-Pb	272±3	Bi et al., 2016
21	Hongqi	Monzogranite	*	LA-ICP-MS zircon U-Pb	267±2	Bi et al., 2016
22	Yifenchang	Monzogranite	*	LA-ICP-MS zircon U-Pb	301±2	Bi et al., 2016
23	Sifenchang	Monzogranite	*	LA-ICP-MS zircon U-Pb	302±3	Bi et al., 2016
24	Suolun	Monzogranite	*	LA-ICP-MS zircon U-Pb	282±2	Bi et al., 2016
25	Tuanshan	Granodiorite	*	LA-ICP-MS zircon U-Pb	287±3	Bi et al., 2016
26	Jianchazhan	Granodiorite	*	LA-ICP-MS zircon U-Pb	302±4	Bi et al., 2016
27	Fangshan	Monzogranite	*	LA-ICP-MS zircon U-Pb	281±2	Bi et al., 2016
28	Yingchun	Granodiorite	*	LA-ICP-MS zircon U-Pb	293±2	Bi et al., 2016
29	Baoqing	Rhyolite	Haojiatun	LA-ICP-MS zircon U-Pb	291±2	Meng et al., 2008
30		Dacite	Haojiatun	LA-ICP-MS zircon U-Pb	286±3	Meng et al., 2008
31		Rhyolitic welded tuff	Dongshan	LA-ICP-MS zircon U-Pb	263±2	Meng et al., 2008
32		Dacite	Dongshan	LA-ICP-MS zircon U-Pb	288±2	Meng et al., 2008
33		Dacite	Zhenzishan	LA-ICP-MS zircon U-Pb	263±5	Meng et al., 2008
34		Basalt-andesite	Erlongshan	LA-ICP-MS zircon U-Pb	293±2	Meng et al., 2008
35		Basalt-andesite	Haojiatun	LA-ICP-MS zircon U-Pb	275±3	Bi et al., 2017
36		Rhyolitic crystal tuf	Haojiatun	LA-ICP-MS zircon U-Pb	290±2	Bi et al., 2017
37	Yanggang	Rhtolitic porphyry	Yanggang	LA-ICP-MS zircon U-Pb	264±7	Meng et al., 2008
38		Rhyolite	Yanggang	LA-ICP-MS zircon U-Pb	268±2	Meng et al., 2008
39	Jiejinkou-Qindeli	Meta-rhyolite	Dalingqiao	LA-ICP-MS zircon U-Pb	279±2	Bi et al., 2017
40		Rhyolite	Dalingqiao	LA-ICP-MS zircon U-Pb	279±5	Bi et al., 2017
41		Metabasalt	*	LA-ICP-MS zircon U-Pb	275±6	Unpublished data
42	Longtouqiao	Rhyolite	Zhenzishan	LA-ICP-MS zircon U-Pb	267±5	Bi et al., 2017
43		Rhyolitic crystal tuff	Zhenzishan	LA-ICP-MS zircon U-Pb	269±3	Bi et al., 2017

were 32 μm in diameter. U, Th and Pb concentrations were calibrated using ^{29}Si as an internal standard. The standard zircon 91500 (Wiedenbeck et al., 1995) was used as an external standard to normalize isotopic fractionation during analysis. Analytical procedures used follow those described by Yuan et al. (2004). Raw data were processed using the GLITTER program. Uncertainties of individual analyses are reported with 1σ error; weighted mean ages were calculated at 1σ confidence level. The data were processed using the ISOPLOT (Version 3.0) program (Ludwig, 2003). The zircon Plešovice was dated as an unknown sample and yielded a weighted mean $^{206}Pb/^{238}U$ age of 337.5±2.4 Ma (n=8, 2σ), which is in good agreement with the recommended age of 337.13±0.37 Ma (Sláma et al., 2008) The dating results are given in Table 2.

3.2 Hf isotope analysis

In-situ zircon Lu-Hf isotope analyses were conducted using a Neptune multi-collector ICP–MS (MC-LA-ICPMS) (Thermo Fisher Scientific, Germany) in combination with a Geolas 2005 excimer ArF laser ablation system (193 nm) that is housed within the Institute of Geology and Geophysics, Chinese Academy of Sciences, Beijing, China. The analysis spots were 44 μm in diameter. The ablated aerosol was carried by helium, and 91500 served as the external standard. For details of the operating conditions for the laser ablation system and the MC-ICP-MS instrument, as well as the analytical method, see Xu et al. (2004) and Wu et al. (2006). Interference of ^{176}Yb on ^{176}Hf was corrected by measuring the interference-free ^{172}Yb isotope and using $^{176}Lu/^{172}Yb$ = 0.5886 (Wu et al., 2006). Similarly, the relatively minor interference of ^{176}Lu on ^{176}Hf was corrected by measuring the intensity of the interference-free ^{175}Lu isotope and using the recommended $^{176}Lu/^{175}Lu$ = 0.02655 (Machado and Simonetti, 2001) to calculate $^{176}Lu/^{177}Hf$ ratios. Hf model ages were calculated using equations derived by Griffin et al. (2000) and Wu et al. (2007). The Hf isotope data are given in Table 3.

4 Analytical Results

4.1 Zircon U-Pb results

The selected zircons are columnar, colorless and transparent grains with a particle size of about 50-140 μm. And some of zircons are equiaxial and about 40-60 μm (Fig. 6). The CL imaging reveal that most of the zircon grains show oscillation zones, with their high Th/U ratios (Table 2), indicating that most zircons are magmatic origin (Koschek et al., 1993; Belousova et al., 2002; Wu et al., 2004).

A total of 66 U-Pb analyses, in sample 14H13-3, were

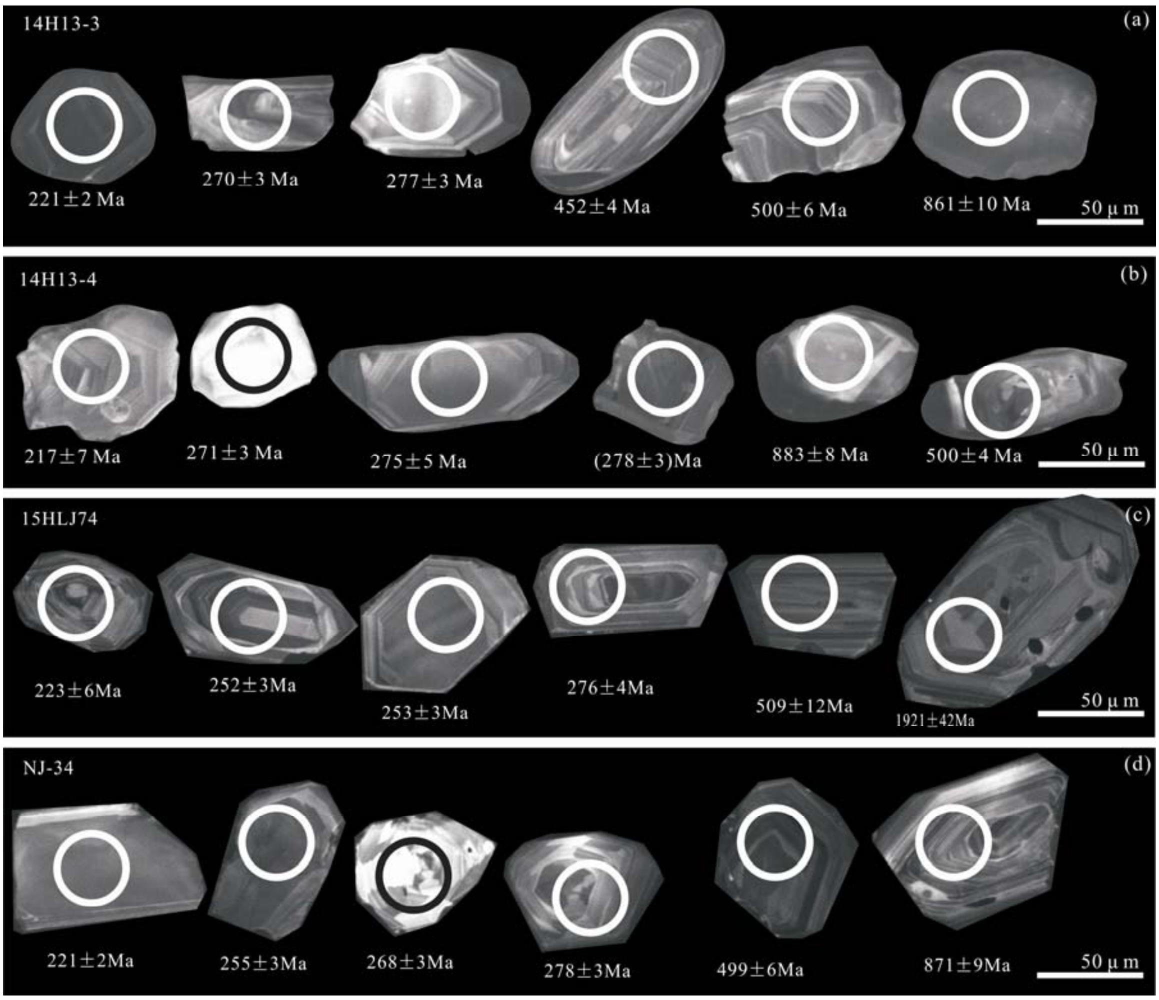

Fig. 6. CL images of the selected zircons from the Nanshuangyashan Formation.

Table 2 LA–ICP–MS U–Pb data for zircons from the Nanshuangyashan Formation in the eastern part of the Jiamusi Massif

Analysis	Element content (ppm)			Th/U	Isotopic ratios						Age (Ma)						Concordance
	Pb	Th	U		^{207}Pb/^{206}Pb	1σ	^{207}Pb/^{235}U	1σ	^{206}Pb/^{238}U	1σ	^{207}Pb/^{206}Pb	1σ	^{207}Pb/^{235}U	1σ	^{206}Pb/^{238}U	1σ	
14H13-3 (63 analyses)																	
1	160	1554	2902	0.54	0.0610	0.0089	0.2708	0.0103	0.0352	0.0010	639	312	243	8	223	6	91%
2	55.1	421	772	0.55	0.0539	0.0019	0.3304	0.0120	0.0443	0.0012	365	80	290	9	279	7	96%
3	98	498	626	0.80	0.0575	0.0020	0.6077	0.0210	0.0764	0.0021	522	76	482	13	474	12	98%
4	289	1614	2086	0.77	0.0577	0.0018	0.6178	0.0196	0.0774	0.0021	520	69	488	12	481	13	98%
5	61.2	255	604	0.42	0.0563	0.0020	0.6018	0.0215	0.0775	0.0021	465	80	478	14	481	13	99%
6	110	1051	1394	0.75	0.0522	0.0018	0.3127	0.0111	0.0434	0.0012	300	78	276	9	274	8	99%
7	335	1540	3252	0.47	0.0563	0.0018	0.6158	0.0205	0.0791	0.0022	465	105	487	13	491	13	99%
8	59.8	414	988	0.42	0.0553	0.0020	0.3379	0.0126	0.0442	0.0012	433	81	296	10	279	8	94%
9	36.1	352	626	0.56	0.0544	0.0021	0.2555	0.0098	0.0340	0.0009	387	85	231	8	216	6	93%
10	147	1823	1076	1.69	0.0533	0.0019	0.2964	0.0104	0.0403	0.0011	343	80	264	8	255	7	96%
11	53.6	221	511	0.43	0.0574	0.0020	0.6290	0.0221	0.0795	0.0022	506	78	495	14	493	13	99%
12	95	789	1476	0.53	0.0530	0.0019	0.3133	0.0111	0.0427	0.0012	328	75	277	9	270	7	97%
13	24.3	57.9	805	0.07	0.0576	0.0028	0.3063	0.0146	0.0390	0.0012	522	75	271	11	247	7	90%
14	66.2	114	141	0.81	0.0883	0.0032	2.9761	0.1084	0.2436	0.0069	1391	69	1402	28	1405	36	99%
15	49.2	193	498	0.39	0.0584	0.0021	0.6254	0.0225	0.0775	0.0022	543	78	493	14	481	13	97%
16	71	719	592	1.21	0.0526	0.0020	0.3006	0.0114	0.0413	0.0012	322	81	267	9	261	7	97%
17	138	497	1239	0.40	0.0617	0.0022	0.6735	0.0227	0.0792	0.0022	661	79	523	14	491	13	93%
18	77	819	793	1.03	0.0532	0.0020	0.3029	0.0114	0.0411	0.0012	339	92	269	9	260	7	96%
19	56.9	270	397	0.68	0.0582	0.0021	0.6483	0.0239	0.0806	0.0024	600	78	507	15	500	14	98%
20	74	684	984	0.70	0.0541	0.0018	0.3120	0.0106	0.0417	0.0012	376	76	276	8	263	7	95%
21	44.8	366	686	0.53	0.0512	0.0019	0.3025	0.0111	0.0428	0.0012	250	85	268	9	270	7	99%
22	221	994	2056	0.48	0.0570	0.0018	0.6189	0.0194	0.0785	0.0021	500	70	489	12	487	13	99%
23	68.2	285	627	0.46	0.0567	0.0021	0.6259	0.0224	0.0801	0.0023	480	86	494	14	497	14	99%
24	42.4	358	565	0.63	0.0538	0.0021	0.3241	0.0122	0.0436	0.0012	365	87	285	9	275	8	96%
26	24.0	232	206	1.13	0.0548	0.0025	0.3366	0.0156	0.0447	0.0013	406	104	295	12	282	8	95%
27	48.2	452	861	0.53	0.0525	0.0025	0.2562	0.0092	0.0347	0.0010	306	106	232	7	220	6	94%
28	49.2	276	216	1.28	0.0591	0.0023	0.6536	0.0245	0.0804	0.0023	572	85	511	15	498	13	97%
29	148	602	1371	0.44	0.0556	0.0017	0.6057	0.0198	0.0789	0.0023	435	69	481	13	489	13	98%
30	32.7	129	353	0.37	0.0555	0.0020	0.6123	0.0227	0.0801	0.0024	432	80	485	14	497	14	97%
31	75.0	307	617	0.50	0.0557	0.0019	0.6195	0.0216	0.0805	0.0023	443	79	490	14	499	14	98%
32	32.1	306	393	0.78	0.0509	0.0020	0.2976	0.0117	0.0426	0.0013	235	89	265	9	269	8	98%
33	77	340	579	0.59	0.0578	0.0020	0.6451	0.0225	0.0810	0.0023	520	69	505	14	502	14	99%
34	43.4	518	496	1.04	0.0502	0.0028	0.2403	0.0132	0.0348	0.0010	211	125	219	11	221	6	99%
35	62.0	538	771	0.70	0.0527	0.0019	0.3065	0.0113	0.0421	0.0012	322	81	271	9	266	7	97%
36	16.9	150	253	0.60	0.0520	0.0024	0.2951	0.0133	0.0413	0.0012	287	101	263	10	261	7	99%
37	61.7	247	622	0.40	0.0562	0.0020	0.6158	0.0224	0.0793	0.0023	461	75	487	14	492	13	98%
38	276	1434	1843	0.78	0.0586	0.0019	0.6432	0.0215	0.0794	0.0022	554	70	504	13	492	13	97%
39	47.4	460	884	0.52	0.0519	0.0018	0.2503	0.0087	0.0349	0.0010	283	78	227	7	221	6	97%
40	57.4	615	404	1.52	0.0537	0.0021	0.3101	0.0129	0.0417	0.0012	361	61	274	10	264	7	96%
41	174	678	1657	0.41	0.0561	0.0018	0.6176	0.0212	0.0796	0.0022	457	70	488	13	494	13	98%
42	67.5	610	849	0.72	0.0529	0.0019	0.3115	0.0111	0.0428	0.0012	324	112	275	9	270	7	98%
43	33.2	52.0	71.3	0.73	0.0867	0.0030	2.9442	0.1059	0.2461	0.0072	1354	67	1393	27	1419	37	98%
44	53.0	468	620	0.76	0.0554	0.0031	0.3202	0.0173	0.0421	0.0012	432	124	282	13	266	8	93%
45	11.6	142	142	1.00	0.0519	0.0031	0.2418	0.0143	0.0341	0.0010	280	106	220	12	216	6	98%
47	184	861	1637	0.53	0.0510	0.0024	0.5416	0.0240	0.0764	0.0024	239	109	439	16	474	14	92%
48	25.2	118	169	0.70	0.0551	0.0024	0.6049	0.0243	0.0800	0.0024	417	103	480	15	496	14	96%
49	135	570	1134	0.50	0.0567	0.0019	0.6287	0.0203	0.0801	0.0023	480	74	495	13	497	14	99%
50	108	1301	592	2.20	0.0540	0.0020	0.3095	0.0112	0.0414	0.0012	372	83	274	9	262	7	95%
51	95	441	698	0.63	0.0566	0.0018	0.6187	0.0198	0.0792	0.0023	476	38	489	12	492	14	99%
52	70.1	143	454	0.32	0.0687	0.0023	1.2646	0.0434	0.1330	0.0038	900	73	830	19	805	21	96%
53	104	236	522	0.45	0.0678	0.0022	1.2668	0.0488	0.1349	0.0044	865	69	831	22	816	25	98%
54	108	280	501	0.56	0.0755	0.0026	1.3918	0.0540	0.1338	0.0045	1083	70	885	23	809	26	91%
55	122	1443	969	1.49	0.0542	0.0028	0.3143	0.0171	0.0419	0.0013	389	119	277	13	265	8	95%
57	39.6	183	305	0.60	0.0570	0.0020	0.6452	0.0237	0.0819	0.0023	500	80	506	15	507	14	99%
58	236	831	2609	0.32	0.0568	0.0018	0.6396	0.0205	0.0813	0.0023	483	70	502	13	504	14	99%
59	63.5	71.7	1286	0.06	0.0573	0.0020	0.6399	0.0228	0.0809	0.0024	502	78	502	14	502	14	99%
60	67.1	297	431	0.69	0.0637	0.0023	0.6998	0.0269	0.0790	0.0023	731	78	539	16	490	14	90%
61	54.5	188	468	0.40	0.0619	0.0022	0.7420	0.0271	0.0866	0.0026	672	78	564	16	536	15	94%
62	98	465	703	0.66	0.0575	0.0020	0.6191	0.0209	0.0779	0.0022	522	78	489	13	483	13	98%
63	116	1073	1351	0.79	0.0529	0.0018	0.3096	0.0108	0.0423	0.0012	328	106	274	8	267	8	97%
64	152	241	181	1.33	0.1035	0.0033	4.0392	0.1302	0.2829	0.0082	1687	59	1642	26	1606	41	97%
65	12.4	105	182	0.58	0.0510	0.0026	0.2925	0.0156	0.0416	0.0013	239	119	261	12	263	8	99%
66	48.3	604	420	1.44	0.0493	0.0022	0.2366	0.0109	0.0347	0.0011	161	102	216	9	220	7	97%
14H13-4 (60 analyses)																	
1	60.0	436	1089	0.40	0.0526	0.0018	0.3078	0.0108	0.0423	0.0012	309	80	272	8	267	7	98%
2	37.6	312	536	0.58	0.0506	0.0020	0.3027	0.0119	0.0433	0.0013	220	89	269	9	273	8	98%
3	55.7	447	831	0.54	0.0538	0.0019	0.3238	0.0115	0.0434	0.0012	361	78	285	9	274	8	96%

Continued Table 2

Analysis	Element content (ppm)			Th/U	Isotopic ratios						Age (Ma)						Concordance
	Pb	Th	U		$^{207}Pb/^{206}Pb$	1σ	$^{207}Pb/^{235}U$	1σ	$^{206}Pb/^{238}U$	1σ	$^{207}Pb/^{206}Pb$	1σ	$^{207}Pb/^{235}U$	1σ	$^{206}Pb/^{238}U$	1σ	
4	10.4	117	179	0.66	0.0527	0.0030	0.2523	0.0140	0.0347	0.0010	322	125	228	11	220	6	96%
5	46.5	333	746	0.45	0.0533	0.0021	0.3280	0.0120	0.0445	0.0012	343	87	288	9	281	8	97%
7	64.8	317	426	0.74	0.0570	0.0022	0.6533	0.0251	0.0823	0.0024	500	83	511	15	510	15	99%
8	62.2	476	1002	0.48	0.0528	0.0018	0.3212	0.0110	0.0438	0.0012	324	78	283	8	276	8	97%
9	33.7	305	344	0.89	0.0528	0.0021	0.3199	0.0122	0.0440	0.0013	320	88	282	9	278	8	98%
10	8.3	96.9	107	0.91	0.0475	0.0031	0.2246	0.0147	0.0343	0.0010	76.0	157	206	12	217	6	94%
11	18.0	137	270	0.51	0.0523	0.0023	0.3270	0.0144	0.0452	0.0013	298	100	287	11	285	8	99%
12	5.84	27.5	43.2	0.64	0.0618	0.0042	0.6807	0.0437	0.0809	0.0027	733	144	527	26	501	16	94%
13	208	1100	1458	0.75	0.0581	0.0020	0.6344	0.0224	0.0788	0.0022	600	76	499	14	489	13	98%
14	286	1278	2594	0.49	0.0572	0.0018	0.6281	0.0203	0.0794	0.0022	498	68	495	13	493	13	99%
15	42.7	391	488	0.80	0.0510	0.0020	0.2923	0.0118	0.0415	0.0012	239	93	260	9	262	7	99%
16	55.4	485	792	0.61	0.0527	0.0019	0.3039	0.0110	0.0418	0.0012	322	83	269	9	264	7	97%
17	84	726	1288	0.56	0.0533	0.0019	0.3096	0.0110	0.0420	0.0012	343	80	274	9	265	7	96%
18	154	512	1906	0.27	0.0582	0.0020	0.6391	0.0221	0.0796	0.0023	600	74	502	14	494	14	98%
19	31.6	229	424	0.54	0.0560	0.0023	0.3441	0.0138	0.0447	0.0013	454	86	300	10	282	8	93%
20	39.4	381	398	0.96	0.0517	0.0020	0.3026	0.0122	0.0424	0.0012	272	86	268	9	268	8	99%
21	81	758	1101	0.69	0.0506	0.0018	0.2932	0.0106	0.0421	0.0012	220	51	261	8	266	7	98%
22	11.4	130	187	0.70	0.0522	0.0027	0.2463	0.0128	0.0342	0.0010	295	119	224	10	216	6	96%
23	23.3	229	204	1.13	0.0527	0.0026	0.3244	0.0152	0.0449	0.0013	317	111	285	12	283	8	99%
24	43.7	365	650	0.56	0.0518	0.0021	0.2933	0.0119	0.0411	0.0012	280	93	261	9	259	7	99%
25	121	311	567	0.55	0.0686	0.0024	1.2782	0.0450	0.1348	0.0037	887	77	836	20	815	21	97%
26	29.1	323	400	0.81	0.0507	0.0020	0.2472	0.0104	0.0352	0.0010	228	58	224	9	223	6	99%
27	59.7	493	912	0.54	0.0528	0.0020	0.3018	0.0112	0.0413	0.0011	320	116	268	9	261	7	97%
28	147	1527	1623	0.94	0.0534	0.0018	0.3061	0.0106	0.0416	0.0012	343	78	271	8	262	7	96%
29	40.2	371	520	0.71	0.0574	0.0032	0.3380	0.0189	0.0426	0.0013	506	116	296	14	269	8	90%
30	55.1	243	433	0.56	0.0612	0.0023	0.6830	0.0264	0.0809	0.0025	656	81	529	16	501	15	94%
31	57.2	440	736	0.60	0.0558	0.0021	0.3419	0.0138	0.0442	0.0013	443	85	299	10	279	8	93%
32	88	235	329	0.71	0.0700	0.0024	1.4015	0.0503	0.1449	0.0043	929	70	890	21	872	24	98%
33	57.8	584	514	1.14	0.0551	0.0022	0.3138	0.0124	0.0413	0.0012	417	91	277	10	261	7	93%
34	97	1105	742	1.49	0.0517	0.0019	0.2984	0.0111	0.0419	0.0012	272	92	265	9	264	7	99%
35	70.6	635	861	0.74	0.0535	0.0020	0.3094	0.0114	0.0419	0.0012	350	85	274	9	265	7	96%
36	10.6	129	139	0.93	0.0518	0.0034	0.2422	0.0160	0.0341	0.0011	276	150	220	13	216	7	98%
37	86.2	297	1053	0.28	0.0560	0.0019	0.6136	0.0208	0.0792	0.0022	454	74	486	13	491	13	98%
39	53.2	459	707	0.65	0.0529	0.0020	0.3069	0.0116	0.0420	0.0012	328	85	272	9	265	7	97%
40	81.9	323	1057	0.31	0.0629	0.0023	0.6736	0.0281	0.0770	0.0022	706	74	523	17	478	13	91%
41	66	661	524	1.26	0.0526	0.0023	0.3018	0.0132	0.0415	0.0012	322	98	268	10	262	8	97%
42	112	496	829	0.60	0.0604	0.0022	0.6526	0.0228	0.0785	0.0022	617	78	510	14	487	13	95%
43	93	842	1250	0.67	0.0543	0.0019	0.3129	0.0108	0.0418	0.0011	383	78	276	8	264	7	95%
44	8.3	39.9	50.8	0.79	0.0612	0.0034	0.6907	0.0378	0.0823	0.0024	656	119	533	23	510	15	95%
45	73.4	666	1000	0.67	0.0539	0.0018	0.3240	0.0115	0.0436	0.0013	369	71	285	9	275	8	96%
47	67.1	535	946	0.57	0.0547	0.0020	0.3244	0.0126	0.0430	0.0012	398	79	285	10	271	8	95%
49	35.2	120	402	0.30	0.0579	0.0020	0.6412	0.0235	0.0805	0.0023	524	78	503	15	499	14	99%
50	81	766	1016	0.75	0.0540	0.0018	0.3122	0.0104	0.0421	0.0012	372	81	276	8	266	7	96%
51	10.9	119	181	0.66	0.0548	0.0029	0.2583	0.0137	0.0345	0.0010	406	117	233	11	219	6	93%
52	14.6	106	233	0.46	0.0518	0.0023	0.3226	0.0148	0.0453	0.0014	276	100	284	11	286	8	99%
53	71	644	815	0.79	0.0546	0.0019	0.3149	0.0116	0.0418	0.0012	398	80	278	9	264	7	94%
54	78.0	77.8	1564	0.05	0.0589	0.0018	0.6495	0.0212	0.0799	0.0022	565	69	508	13	495	13	97%
56	111	1152	1162	0.99	0.0507	0.0022	0.2939	0.0134	0.0426	0.0013	228	100	262	11	269	8	97%
57	40.5	332	561	0.59	0.0533	0.0020	0.3087	0.0119	0.0422	0.0012	343	90	273	9	266	8	97%
58	26.4	205	428	0.48	0.0530	0.0021	0.3064	0.0128	0.0420	0.0013	332	91	271	10	265	8	97%
59	25.0	238	342	0.70	0.0492	0.0023	0.2800	0.0132	0.0415	0.0013	167	105	251	10	262	8	95%
60	105	925	1405	0.66	0.0538	0.0022	0.3165	0.0129	0.0428	0.0012	365	60	279	10	270	8	96%
61	41.4	348	573	0.61	0.0511	0.0020	0.3027	0.0122	0.0429	0.0012	243	91	269	9	271	7	99%
62	54.8	467	685	0.68	0.0514	0.0019	0.3006	0.0119	0.0424	0.0013	257	87	267	9	268	8	99%
63	42.6	342	579	0.59	0.0541	0.0021	0.3246	0.0130	0.0436	0.0013	372	87	285	10	275	8	96%
64	41.4	349	561	0.62	0.0534	0.0020	0.3033	0.0117	0.0413	0.0013	346	87	269	9	261	8	96%
65	31.3	257	404	0.64	0.0519	0.0021	0.3138	0.0128	0.0441	0.0014	280	92	277	10	278	9	99%
15HLJ74（94 analyses）																	
2	196	46.6	469	0.10	0.1176	0.0038	5.3925	0.1731	0.3305	0.0087	1921	57	1884	28	1841	42	97%
3	440	109	1022	0.11	0.1156	0.0036	5.3644	0.1701	0.3344	0.0089	1889	56	1879	27	1860	43	98%
4	171	380	837	0.45	0.0563	0.0019	0.6287	0.0214	0.0806	0.0021	461	108	495	13	500	13	99%
5	59.2	145	239	0.61	0.0555	0.0023	0.6236	0.0255	0.0813	0.0022	435	93	492	16	504	13	97%
6	82	424	592	0.72	0.0539	0.0024	0.2862	0.0121	0.0386	0.0010	365	98	256	10	244	6	95%
7	73.2	64.3	211	0.31	0.0716	0.0026	1.6834	0.0617	0.1697	0.0046	973	79	1002	23	1011	25	99%
8	177	110	136	0.80	0.1088	0.0037	5.0038	0.1749	0.3312	0.0090	1789	62	1820	30	1844	44	98%
9	145	270	657	0.41	0.0642	0.0025	0.7796	0.0303	0.0879	0.0024	750	81	585	17	543	14	92%
10	125	160	949	0.17	0.0616	0.0023	0.6855	0.0252	0.0800	0.0021	661	75	530	15	496	12	93%
11	163	360	880	0.41	0.0603	0.0034	0.6662	0.0266	0.0814	0.0023	617	129	518	16	504	14	97%

Continued Table 2

Analysis	Element content (ppm)			Th/U	Isotopic ratios						Age (Ma)						Concordance
	Pb	Th	U		$^{207}Pb/^{206}Pb$	1σ	$^{207}Pb/^{235}U$	1σ	$^{206}Pb/^{238}U$	1σ	$^{207}Pb/^{206}Pb$	1σ	$^{207}Pb/^{235}U$	1σ	$^{206}Pb/^{238}U$	1σ	
12	204	252	531	0.47	0.0702	0.0023	1.4261	0.0455	0.1465	0.0038	933	67	900	19	881	21	97%
13	40.2	170	372	0.46	0.0512	0.0028	0.2886	0.0159	0.0405	0.0011	250	126	257	13	256	7	99%
14	157	287	964	0.30	0.0605	0.0022	0.6992	0.0246	0.0834	0.0022	620	76	538	15	516	13	95%
15	128	643	739	0.87	0.0517	0.0021	0.2916	0.0117	0.0407	0.0011	272	94	260	9	257	7	99%
16	57.7	217	444	0.49	0.0530	0.0027	0.3288	0.0166	0.0450	0.0012	328	119	289	13	284	8	98%
17	48.9	101	247	0.41	0.0580	0.0024	0.6832	0.0285	0.0854	0.0023	528	91	529	17	528	14	99%
18	99	247	266	0.93	0.0594	0.0026	0.6656	0.0286	0.0813	0.0022	583	95	518	17	504	13	97%
19	144	181	243	0.74	0.0714	0.0028	1.4450	0.0588	0.1455	0.0040	970	78	908	24	876	23	96%
20	82	442	326	1.35	0.0506	0.0024	0.2828	0.0135	0.0406	0.0011	220	113	253	11	257	7	98%
21	74	166	331	0.50	0.0585	0.0024	0.6501	0.0260	0.0810	0.0022	550	89	509	16	502	13	98%
22	11.2	53.8	62.6	0.86	0.0525	0.0071	0.3302	0.0420	0.0456	0.0016	306	281	290	32	287	10	99%
23	53.6	259	444	0.58	0.0534	0.0023	0.2873	0.0126	0.0390	0.0011	346	98	256	10	247	7	96%
24	77	200	266	0.75	0.0599	0.0031	0.6595	0.0362	0.0800	0.0023	598	111	514	22	496	14	96%
25	154	297	972	0.31	0.0545	0.0019	0.6202	0.0216	0.0822	0.0022	391	78	490	14	509	13	96%
26	384	975	1012	0.96	0.0582	0.0021	0.6688	0.0230	0.0834	0.0022	539	80	520	14	517	13	99%
27	117	100	125	0.80	0.0868	0.0030	2.9485	0.1020	0.2459	0.0065	1367	67	1394	26	1418	34	98%
28	41.6	95.1	208	0.46	0.0517	0.0026	0.5758	0.0296	0.0804	0.0022	333	119	462	19	499	13	92%
29	27.4	118	217	0.54	0.0488	0.0038	0.2662	0.0195	0.0409	0.0012	139	183	240	16	258	7	92%
30	638	282	381	0.74	0.1472	0.0048	9.7420	0.3177	0.4774	0.0124	2313	56	2411	30	2516	54	95%
31	84	439	367	1.19	0.0551	0.0030	0.3042	0.0153	0.0406	0.0011	417	156	270	12	256	7	94%
32	50.6	206	381	0.54	0.0468	0.0026	0.2273	0.0129	0.0351	0.0010	39.0	130	208	11	223	6	93%
33	153	754	1293	0.58	0.0541	0.0020	0.2938	0.0107	0.0394	0.0011	372	77	262	8	249	7	95%
34	67	318	491	0.65	0.0575	0.0028	0.3193	0.0153	0.0403	0.0011	509	107	281	12	255	7	90%
35	7.2	34.2	44.3	0.77	0.0624	0.0147	0.2850	0.0623	0.0407	0.0016	687	518	255	49	257	10	99%
36	168	1056	1301	0.81	0.0552	0.0024	0.3163	0.0124	0.0418	0.0011	420	101	279	10	264	7	94%
38	370	179	475	0.38	0.1242	0.0039	6.1975	0.1925	0.3597	0.0094	2018	55	2004	27	1981	44	98%
39	20.7	109	142	0.77	0.0514	0.0051	0.2728	0.0294	0.0388	0.0012	257	231	245	23	245	8	99%
40	233	114	282	0.40	0.1181	0.0037	5.7192	0.1773	0.3493	0.0091	1928	57	1934	27	1931	43	99%
42	183	150	668	0.23	0.0722	0.0024	1.6961	0.0564	0.1694	0.0044	991	68	1007	21	1009	24	99%
43	241	119	313	0.38	0.1185	0.0038	5.5443	0.1818	0.3375	0.0091	1944	58	1907	28	1874	44	98%
44	275	122	439	0.28	0.1159	0.0036	5.4727	0.1705	0.3401	0.0089	1894	56	1896	27	1887	43	99%
45	134	668	913	0.73	0.0535	0.0021	0.2929	0.0117	0.0395	0.0011	350	91	261	9	250	7	95%
46	58.0	133	230	0.58	0.0570	0.0026	0.6558	0.0303	0.0832	0.0023	500	102	512	19	515	13	99%
47	146	115	215	0.54	0.0925	0.0031	3.1088	0.1028	0.2428	0.0065	1477	63	1435	25	1401	33	97%
48	142	174	621	0.28	0.0619	0.0023	0.7781	0.0338	0.0896	0.0028	672	78	584	19	553	16	94%
49	58.3	49.1	117	0.42	0.0807	0.0032	2.3528	0.0972	0.2102	0.0060	1217	74	1228	29	1230	32	99%
50	162	86.8	108	0.81	0.1262	0.0042	6.9426	0.2308	0.3978	0.0107	2046	58	2104	30	2159	49	97%
51	205	47.1	520	0.09	0.1156	0.0035	5.3678	0.1672	0.3353	0.0089	1889	55	1880	27	1864	43	99%
52	70	324	617	0.52	0.0528	0.0022	0.2890	0.0122	0.0396	0.0011	320	96	258	10	250	7	97%
53	44.7	195	281	0.69	0.0548	0.0037	0.3122	0.0221	0.0415	0.0012	406	147	276	17	262	7	94%
54	13.1	48.5	90.3	0.54	0.0547	0.0058	0.3073	0.0333	0.0416	0.0013	398	239	272	26	262	8	96%
55	194	44.7	465	0.10	0.1276	0.0039	5.9296	0.1929	0.3364	0.0093	2065	54	1966	28	1869	45	94%
56	18.1	156	230	0.68	0.0563	0.0018	0.3067	0.0098	0.0395	0.0005	465	105	272	8	250	3	91%
57	44.1	365	564	0.65	0.0494	0.0013	0.2707	0.0074	0.0396	0.0005	165	63	243	6	251	3	97%
58	8.84	62.0	126	0.49	0.0561	0.0045	0.3231	0.0263	0.0415	0.0006	457	150	284	20	262	4	91%
59	5.95	46.3	69.8	0.66	0.0524	0.0031	0.2868	0.0157	0.0401	0.0007	302	135	256	12	253	4	98%
60	39.6	346	483	0.72	0.0543	0.0019	0.3010	0.0120	0.0398	0.0006	383	80	267	9	251	4	93%
61	10.3	75.8	133	0.57	0.0571	0.0037	0.3064	0.0180	0.0397	0.0006	494	144	271	14	251	4	92%
62	12.2	102	159	0.64	0.0508	0.0019	0.2752	0.0100	0.0395	0.0005	232	92	247	8	250	3	98%
63	22.3	194	259	0.75	0.0508	0.0019	0.2751	0.0095	0.0398	0.0006	228	90	247	8	251	4	98%
64	17.2	134	252	0.53	0.0516	0.0017	0.2823	0.0093	0.0397	0.0005	333	76	252	7	251	3	99%
65	30.5	304	298	1.02	0.0528	0.0019	0.2887	0.0101	0.0397	0.0005	320	114	258	8	251	3	97%
66	19.8	162	253	0.64	0.0544	0.0019	0.2941	0.0094	0.0395	0.0005	387	80	262	7	250	3	95%
67	14.5	130	162	0.80	0.0548	0.0022	0.2966	0.0114	0.0397	0.0005	467	95	264	9	251	3	95%
68	20.8	177	249	0.71	0.0555	0.0022	0.2988	0.0104	0.0396	0.0006	432	87	265	8	250	4	94%
69	8.39	63.4	128	0.50	0.0559	0.0027	0.3045	0.0145	0.0396	0.0006	450	107	270	11	250	3	92%
70	18.4	162	221	0.73	0.0524	0.0021	0.2858	0.0115	0.0397	0.0005	302	91	255	9	251	3	98%
71	22.6	183	305	0.60	0.0492	0.0017	0.2703	0.0096	0.0398	0.0005	167	81	243	8	252	3	96%
72	42.9	398	477	0.83	0.0499	0.0013	0.2732	0.0072	0.0398	0.0006	187	64	245	6	252	4	97%
73	26.0	199	372	0.53	0.0531	0.0015	0.2877	0.0075	0.0395	0.0005	332	31	257	6	250	3	97%
74	4.83	28.8	76.3	0.38	0.0533	0.0030	0.2882	0.0169	0.0395	0.0007	343	134	257	13	249	4	96%
75	9.1	67.2	118	0.57	0.0567	0.0027	0.3286	0.0150	0.0425	0.0010	480	108	289	11	269	6	92%
76	6.22	41.4	84.4	0.49	0.0570	0.0031	0.3309	0.0172	0.0425	0.0006	500	119	290	13	268	4	92%
77	19.4	172	219	0.79	0.0515	0.0020	0.2797	0.0103	0.0395	0.0005	265	89	250	8	250	3	99%
78	13.1	104	167	0.62	0.0534	0.0023	0.2903	0.0124	0.0396	0.0006	346	92	259	10	250	3	96%
79	9.8	74.0	134	0.55	0.0555	0.0026	0.3010	0.0141	0.0397	0.0007	435	138	267	11	251	4	93%
80	7.16	51.7	105	0.49	0.0511	0.0028	0.2757	0.0154	0.0394	0.0007	243	121	247	12	249	4	99%
81	9.6	73.8	124	0.60	0.0511	0.0026	0.2741	0.0134	0.0395	0.0006	256	121	246	11	250	4	98%

Continued Table 2

Analysis	Element content (ppm)			Th/U	Isotopic ratios						Age (Ma)						Concordance
	Pb	Th	U		$^{207}Pb/^{206}Pb$	1σ	$^{207}Pb/^{235}U$	1σ	$^{206}Pb/^{238}U$	1σ	$^{207}Pb/^{206}Pb$	1σ	$^{207}Pb/^{235}U$	1σ	$^{206}Pb/^{238}U$	1σ	
82	36.3	328	417	0.79	0.0512	0.0016	0.2787	0.0095	0.0397	0.0006	250	74	250	8	251	4	99%
83	10.1	74.0	133	0.56	0.0563	0.0029	0.3003	0.0153	0.0394	0.0006	461	117	267	12	249	4	93%
84	15.1	121	189	0.64	0.0552	0.0024	0.2991	0.0125	0.0398	0.0006	420	101	266	10	251	3	94%
85	44.8	408	499	0.82	0.0505	0.0012	0.2743	0.0074	0.0395	0.0005	217	53	246	6	250	3	98%
86	28.5	269	307	0.88	0.0535	0.0019	0.2867	0.0097	0.0392	0.0005	350	47	256	8	248	3	96%
87	16.8	134	218	0.61	0.0534	0.0021	0.2857	0.0106	0.0392	0.0005	343	89	255	8	248	3	97%
88	16.2	138	199	0.69	0.0540	0.0022	0.2934	0.0122	0.0394	0.0005	372	91	261	10	249	3	95%
89	11.1	88.4	158	0.56	0.0521	0.0022	0.2808	0.0121	0.0393	0.0005	300	98	251	10	248	3	98%
90	18.2	153	202	0.76	0.0565	0.0020	0.3046	0.0100	0.0397	0.0005	478	78	270	8	251	3	92%
91	23.6	182	332	0.55	0.0531	0.0016	0.2911	0.0084	0.0396	0.0005	332	67	259	7	250	3	96%
92	20.9	169	212	0.80	0.0540	0.0019	0.3207	0.0107	0.0437	0.0007	372	75	282	8	276	4	97%
93	18.1	141	201	0.70	0.0506	0.0019	0.2939	0.0115	0.0422	0.0005	220	89	262	9	267	3	98%
94	15.0	129	171	0.75	0.0507	0.0036	0.2996	0.0232	0.0437	0.0009	233	167	266	18	275	6	96%
95	18.7	160	235	0.68	0.0534	0.0020	0.2946	0.0103	0.0399	0.0005	346	83	262	8	252	3	96%
96	11.9	93.6	157	0.60	0.0521	0.0024	0.2872	0.0137	0.0396	0.0006	287	107	256	11	250	4	97%
97	18.2	151	238	0.63	0.0538	0.0018	0.2971	0.0104	0.0397	0.0004	365	76	264	8	251	3	94%
NJ-34（52 analyses）																	
1	78.1	398	810	0.49	0.0526	0.0027	0.2930	0.0152	0.0407	0.0012	322	121	261	12	257	7	98%
2	62.1	306	717	0.43	0.0515	0.0024	0.2843	0.0137	0.0403	0.0012	261	107	254	11	255	7	99%
3	261	699	1377	0.51	0.0629	0.0023	0.7717	0.0289	0.0890	0.0024	706	78	581	17	550	14	94%
4	147	167	408	0.41	0.0706	0.0029	1.7050	0.0701	0.1755	0.0047	946	83	1010	26	1042	26	96%
5	334	1137	1455	0.78	0.0581	0.0025	0.6527	0.0286	0.0816	0.0023	532	97	510	18	506	13	99%
6	83.5	219	414	0.53	0.0575	0.0032	0.6774	0.0380	0.0862	0.0026	509	122	525	23	533	15	98%
7	209	1013	3276	0.31	0.0540	0.0023	0.2543	0.0119	0.0342	0.0011	372	96	230	10	217	7	94%
8	58.8	236	881	0.27	0.0517	0.0027	0.2959	0.0156	0.0415	0.0011	272	119	263	12	262	7	99%
9	106.9	177	763	0.23	0.0599	0.0025	0.7380	0.0313	0.0892	0.0025	611	89	561	18	551	15	98%
10	607	1623	2478	0.65	0.0585	0.0021	0.7249	0.0274	0.0895	0.0026	550	78	554	16	553	15	99%
11	371	1077	1418	0.76	0.0641	0.0025	0.7931	0.0330	0.0892	0.0025	746	83	593	19	551	15	92%
12	158	245	546	0.45	0.0701	0.0027	1.3390	0.0533	0.1382	0.0040	931	80	863	23	834	23	96%
13	723	1196	2154	0.56	0.0645	0.0022	1.2577	0.0440	0.1407	0.0039	761	73	827	20	849	22	97%
14	108	530	883	0.60	0.0560	0.0027	0.3512	0.0168	0.0454	0.0013	454	110	306	13	286	8	93%
15	213	2188	2369	0.92	0.0567	0.0024	0.3166	0.0131	0.0406	0.0011	480	94	279	10	256	7	91%
16	82.5	178	546	0.33	0.0561	0.0025	0.6313	0.0285	0.0814	0.0023	454	98	497	18	505	14	98%
17	78.0	144	537	0.27	0.0560	0.0026	0.6884	0.0327	0.0891	0.0026	454	104	532	20	550	16	96%
18	147	820	2241	0.37	0.0496	0.0020	0.2339	0.0103	0.0341	0.0011	176	129	213	8	216	7	98%
19	94.9	206	610	0.34	0.0567	0.0026	0.6357	0.0291	0.0814	0.0023	480	100	500	18	504	14	99%
20	93.2	221	574	0.39	0.0540	0.0025	0.6043	0.0292	0.0809	0.0024	372	106	480	19	502	14	95%
21	78.1	191	428	0.45	0.0541	0.0027	0.6077	0.0295	0.0815	0.0023	376	111	482	19	505	14	95%
22	184	892	1935	0.46	0.0523	0.0022	0.3113	0.0147	0.0425	0.0013	298	96	275	11	268	8	97%
23	242	616	1326	0.46	0.0571	0.0022	0.6361	0.0246	0.0802	0.0022	494	83	500	15	497	13	99%
24	209	545	1139	0.48	0.0583	0.0022	0.6507	0.0247	0.0806	0.0023	539	83	509	15	500	14	98%
25	83	438	751	0.58	0.0518	0.0027	0.3103	0.0152	0.0437	0.0013	276	120	274	12	276	8	99%
26	175	856	2012	0.43	0.0542	0.0021	0.3173	0.0118	0.0422	0.0012	389	82	280	9	267	7	95%
27	51.8	115	298	0.39	0.0583	0.0028	0.7019	0.0343	0.0871	0.0025	543	106	540	20	538	15	99%
28	295	1012	4461	0.23	0.0555	0.0019	0.3030	0.0105	0.0395	0.0011	432	80	269	8	249	7	92%
29	115	766	1679	0.46	0.0517	0.0022	0.2419	0.0103	0.0339	0.0010	333	98	220	8	215	6	97%
31	216	416	848	0.49	0.0701	0.0026	1.6317	0.0602	0.1688	0.0046	931	76	983	23	1006	26	97%
32	310	879	1658	0.53	0.0567	0.0021	0.6355	0.0244	0.0812	0.0023	480	83	499	15	503	14	99%
33	175	1016	1540	0.66	0.0526	0.0021	0.3197	0.0133	0.0443	0.0013	309	91	282	10	280	8	99%
34	219	598	1242	0.48	0.0591	0.0022	0.6759	0.0254	0.0827	0.0023	569	81	524	15	512	14	97%
35	130	154	446	0.35	0.0698	0.0027	1.5459	0.0603	0.1606	0.0044	920	86	949	24	960	24	98%
36	168	485	860	0.56	0.0587	0.0024	0.6734	0.0276	0.0830	0.0024	567	89	523	17	514	14	98%
37	399	526	1128	0.47	0.0701	0.0025	1.6485	0.0617	0.1699	0.0049	931	79	989	24	1012	27	97%
38	129	480	2013	0.24	0.0514	0.0021	0.2962	0.0120	0.0416	0.0011	257	93	263	9	263	7	99%
39	60.2	312	657	0.48	0.0503	0.0026	0.2912	0.0153	0.0420	0.0012	209	119	260	12	265	8	97%
40	43.4	281	511	0.55	0.0509	0.0030	0.2440	0.0146	0.0347	0.0011	235	135	222	12	220	7	99%
41	171	782	2148	0.36	0.0539	0.0021	0.3316	0.0142	0.0445	0.0015	365	87	291	11	281	9	96%
42	329	895	1736	0.52	0.0560	0.0022	0.6373	0.0257	0.0820	0.0023	450	89	501	16	508	14	98%
43	138	426	464	0.92	0.0596	0.0028	0.7230	0.0327	0.0884	0.0025	587	102	552	19	546	15	98%
44	70.1	372	695	0.54	0.0488	0.0026	0.2949	0.0159	0.0438	0.0013	200	128	262	13	276	8	94%
45	67.8	584	882	0.66	0.0537	0.0026	0.2563	0.0129	0.0347	0.0010	367	111	232	10	220	6	94%
46	87.5	177	618	0.29	0.0609	0.0027	0.7222	0.0330	0.0858	0.0025	635	94	552	19	531	15	96%
47	71.0	155	501	0.31	0.0584	0.0028	0.6750	0.0330	0.0839	0.0024	546	107	524	20	520	14	99%
48	63.5	326	628	0.52	0.0566	0.0033	0.3173	0.0177	0.0412	0.0012	476	134	280	14	260	8	92%
49	52.9	240	662	0.36	0.0520	0.0028	0.3146	0.0177	0.0436	0.0013	283	156	278	14	275	8	98%
50	46.8	165	326	0.51	0.0576	0.0031	0.6700	0.0391	0.0843	0.0027	522	119	521	24	522	16	99%
51	202	216	715	0.30	0.0691	0.0025	1.6652	0.0667	0.1731	0.0052	902	70	995	25	1029	28	96%
52	133	330	898	0.37	0.0545	0.0023	0.6096	0.0254	0.0807	0.0023	391	94	483	16	500	13	96%
53	70.0	282	958	0.29	0.0528	0.0025	0.3166	0.0155	0.0432	0.0012	320	109	279	12	272	8	97%

Table 3 Lu–Hf isotopic data for zircons from the Nanshuangyashan Formation in the eastern part of the Jiamusi massif

Sample No.	T (Ma)	$^{176}Yb/^{177}Hf$	$^{176}Lu/^{177}Hf$	$^{176}Hf/^{177}Hf(c)$	$2\sigma_m$	$\varepsilon_{Hf}(0)$	$\varepsilon_{Hf}(t)$	2 σ	T_{DM1}(Hf)	T_{DM2}(Hf)	$f_{Lu/Hf}$
HLJ74−1	223	0.062509	0.002400	0.282956	0.000032	6.5	11.1	1.1	436	550	−0.93
HLJ74−20	249	0.075586	0.003058	0.282742	0.000028	−1.1	3.9	1.0	765	1029	−0.91
HLJ74−31	249	0.052219	0.001920	0.282530	0.000033	−8.6	−3.4	1.2	1048	1495	−0.94
HLJ74−18	250	0.060965	0.002368	0.282634	0.000025	−4.9	0.2	0.9	910	1266	−0.93
HLJ74−30	251	0.015027	0.000741	0.282920	0.000023	5.2	10.6	0.8	468	599	−0.98
HLJ74−16	256	0.024985	0.000972	0.282770	0.000042	−0.1	5.4	1.5	683	939	−0.97
HLJ74−14	257	0.062438	0.002399	0.282642	0.000042	−4.6	0.6	1.5	898	1243	−0.93
HLJ74−29	258	0.010966	0.000447	0.282921	0.000021	5.3	10.9	0.8	462	590	−0.99
HLJ74−11	262	0.033057	0.001289	0.282589	0.000022	−6.5	−1.0	0.8	947	1348	−0.96
HLJ74−15	262	0.027800	0.001088	0.282542	0.000023	−8.1	−2.6	0.8	1008	1452	−0.97
HLJ74−27	262	0.019927	0.000852	0.282504	0.000026	−9.5	−3.9	0.9	1054	1533	−0.97
HLJ74−28	264	0.011089	0.000491	0.282474	0.000021	−10.6	−4.8	0.7	1087	1597	−0.99
HLJ74−38	267	0.030465	0.001171	0.282481	0.000023	−10.3	−4.7	0.8	1097	1587	−0.96
HLJ74−22	268	0.040712	0.001758	0.282535	0.000027	−8.4	−2.8	1.0	1037	1471	−0.95
HLJ74−7	269	0.016673	0.000644	0.282454	0.000020	−11.2	−5.5	0.7	1118	1639	−0.98
HLJ74−40	275	0.018623	0.000788	0.282554	0.000022	−7.7	−1.8	0.8	983	1414	−0.98
HLJ74−33	276	0.016987	0.000746	0.282920	0.000024	5.2	11.2	0.8	468	585	−0.98
HLJ74−24	284	0.020801	0.000910	0.282853	0.000021	2.9	8.9	0.7	565	734	−0.97
HLJ74−6	287	0.011646	0.000606	0.282745	0.000032	−1.0	5.2	1.1	712	974	−0.98
HLJ74−17	496	0.011152	0.000583	0.282348	0.000022	−15.0	−4.3	0.8	1263	1736	−0.98
HLJ74−12	499	0.018138	0.000783	0.282449	0.000022	−11.4	−0.7	0.8	1129	1512	−0.98
HLJ74−19	500	0.020638	0.000792	0.282001	0.000042	−27.3	−16.5	1.5	1751	2511	−0.98
HLJ74−25	500	0.033939	0.001439	0.282301	0.000022	−16.7	−6.2	0.8	1360	1858	−0.96
HLJ74−3	502	0.019628	0.000725	0.282333	0.000025	−15.5	−4.7	0.9	1289	1770	−0.98
HLJ74−26	502	0.025532	0.001057	0.282438	0.000023	−11.8	−1.1	0.8	1153	1541	−0.97
HLJ74−5	504	0.039899	0.001410	0.282511	0.000035	−9.2	1.4	1.2	1061	1385	−0.96
HLJ74−10	509	0.019527	0.000740	0.282166	0.000058	−21.4	−10.5	2.0	1521	2138	−0.98
HLJ74−13	515	0.038516	0.001575	0.282455	0.000026	−11.2	−0.4	0.9	1145	1507	−0.95
HLJ74−21	516	0.034620	0.001265	0.282383	0.000022	−13.8	−2.8	0.8	1238	1661	−0.96
HLJ74−9	528	0.015920	0.000600	0.282258	0.000033	−18.2	−6.8	1.2	1389	1920	−0.98
HLJ74−8	553	0.009341	0.000334	0.282273	0.000019	−17.6	−5.6	0.7	1358	1863	−0.99
HLJ74−37	849	0.039315	0.001468	0.281997	0.000022	−27.4	−9.5	0.8	1789	2332	−0.96
HLJ74−36	881	0.029558	0.001141	0.282028	0.000019	−26.3	−7.5	0.7	1730	2233	−0.97
HLJ74−32	1367	0.021676	0.000898	0.281601	0.000018	−41.4	−11.9	0.6	2307	2873	−0.97
HLJ74−35	1889	0.020448	0.000799	0.281589	0.000020	−41.8	−0.8	0.7	2318	2578	−0.98
HLJ74−34	1894	0.030275	0.001171	0.281614	0.000018	−41.0	−0.2	0.6	2306	2550	−0.96
HLJ74−39	1944	0.012591	0.000462	0.281477	0.000017	−45.8	−3.1	0.6	2449	2762	−0.99
HLJ74−4	2018	0.022318	0.000864	0.281595	0.000023	−41.6	2.2	0.8	2314	2493	−0.97
HLJ74−2	2046	0.019867	0.000726	0.281471	0.000019	−46.0	−1.4	0.7	2474	2736	−0.98
HLJ74−23	2313	0.025895	0.000993	0.281064	0.000021	−60.4	−10.3	0.7	3046	3485	−0.97

obtained, and 3 analyses were discarded due to strong discordance. Amongst the 63 concordant analyses, the grains yield apparent ages ranging from 1687±59 to 216±6 Ma (Table 2). In general, the grains define four age populations: at 223–216 Ma (11.1%) with a peak at 219 Ma, 282–247 Ma (36.5%) with a peak at 255 Ma, 536–474 Ma (44.4%) with a peak at 494 Ma, and the 4th age population (9.5%) is older than 805 Ma. The seven youngest grains yield a weighted mean age of 219±5 Ma (MSWD=0.16) and are interpreted to constrain the maximum depositional age of the sandstone (Figs. 7a, 7b).

A total of 65 U-Pb analyses, in sample 14H13-4, were obtained, and 5 analyses were discarded due to strong discordance. Amongst the 60 concordant analyses, the grains yield apparent ages ranging from 872±24 to 216±6 Ma (Table 2). In general, the grains define four age populations: at 223–216 Ma (8.3%) with a peak at 218 Ma, 286–259 Ma (68.3%) with a peak at 269 Ma, 510–478 Ma (20.3%) with a peak at 499 Ma, and the 4th age population (3.3%) is older than 815 Ma of Precambrian. The six youngest grains yield a weighted mean age of 219±6 Ma (MSWD=0.13) and are interpreted to constrain the maximum depositional age of the sandstone (Figs. 7c, 7d).

A total of 97 U-Pb analyses, in sample 15HLJ74, were obtained, and 3 analyses were discarded due to strong discordance. Amongst the 94 concordant analyses, the grains yield apparent ages ranging from 2313±56 to 223±6 Ma (Table 2). In general, the grains define four age populations: the 1st age population only contains one zircon grain with 223±6 Ma, 287–244 Ma (62.5%) with a peak at 250 Ma, 553–496 Ma (15.6%) with a peak at 509 Ma, and the 4th age population is older than 876 Ma. One youngest grains yield a weighted mean age of 223±6 Ma and are interpreted to constrain the maximum depositional age of the sandstone (Figs. 7e–f).

A total of 53 U-Pb analyses, in sample NJ-34, were obtained, and one analyses was discarded due to strong discordance. Amongst the 52 concordant analyses, the grains yield apparent ages ranging from 1042±26 to 215±6 Ma (Table 2). In general, the grains define four age populations: at 220–215 Ma (9.4%) with a peak at 218 Ma, 286–249 Ma (32.1%) with a peak at 268 Ma, 553–497 Ma (43.39%) with a peak at 510 Ma, and the 4th age population is older than 834 Ma. The five youngest grains yield a weighted mean age of 218±6 Ma (MSWD=0.102) and are interpreted to constrain the maximum depositional age of the sandstone (Figs. 7g–h).

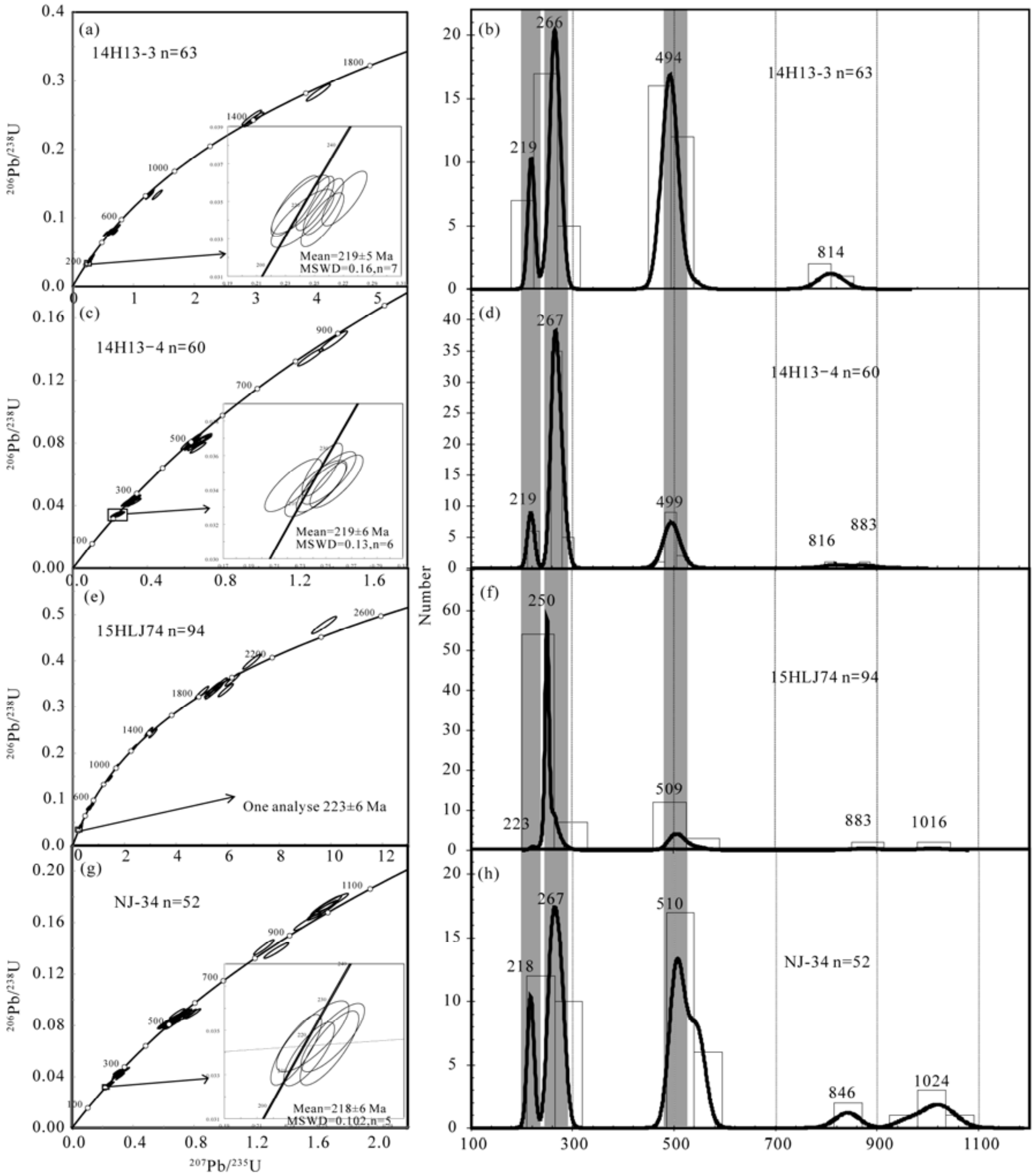
Fig. 7. U-Pb concordia diagrams summarizing the LA-ICP-MS zircon data for the Nanshuangyashan Formation.

4.2 Zircon Hf isotopes

A total of 40 zircons with determined U-Pb ages, representative of the different age groups from sample 15HLJ74, were analysed for their Lu-Hf isotopic compositions. The detrital zircons are characterized by highly variable Lu-Hf isotopic compositions, with $\varepsilon_{\mathrm{Hf}}(t)$ values ranging from negative to positive within a single age group (Fig. 8). The ^{176}Hf/^{177}Hf ratios range from 0.281064 to 0.282956, corresponding to $\varepsilon_{\mathrm{Hf}}(t)$ values，Hf single-stage and two-stage model ages (T_{DM1} and T_{DM2}) range from −16.5 to +11.2, from 3.05 to 0.44 Ga, and from 3.49 to 0.55 Ga, respectively. The detrital zircons show four age populations: >800, 553–496, 287–249 and 223 Ma, which have the $\varepsilon_{\mathrm{Hf}}(t)$ values of –11.9 to +2.2, –16.5 to +1.4, –5.5 to +11.2, and +11.1, respectively (Table 3; Fig. 8). Combined with published data (Cao et al., 2011; Yu et al., 2013a; Bi et al., 2014, 2015, 2016, 2017; Yang et al., 2015; Ge et al., 2017), the analysed zircons of 287–249 and 223–215 Ma mostly have similar Hf isotopic compositions to those of zircons in the CAOB (Xiao et al., 2004 et al., Li et al., 2014, 2016, 2017), but they differ from those of the Neoarchean and Paleoproterozoic zircons in the Paleozoic–Late Mesozoic strata of the Yanshan Fold and Thrust Belt (Yang et al., 2006). the analysed zircons of 553–496 Ma in 15HLJ74 are similar to ca. 492 Ma primary zircons from the monzogranite (Luan

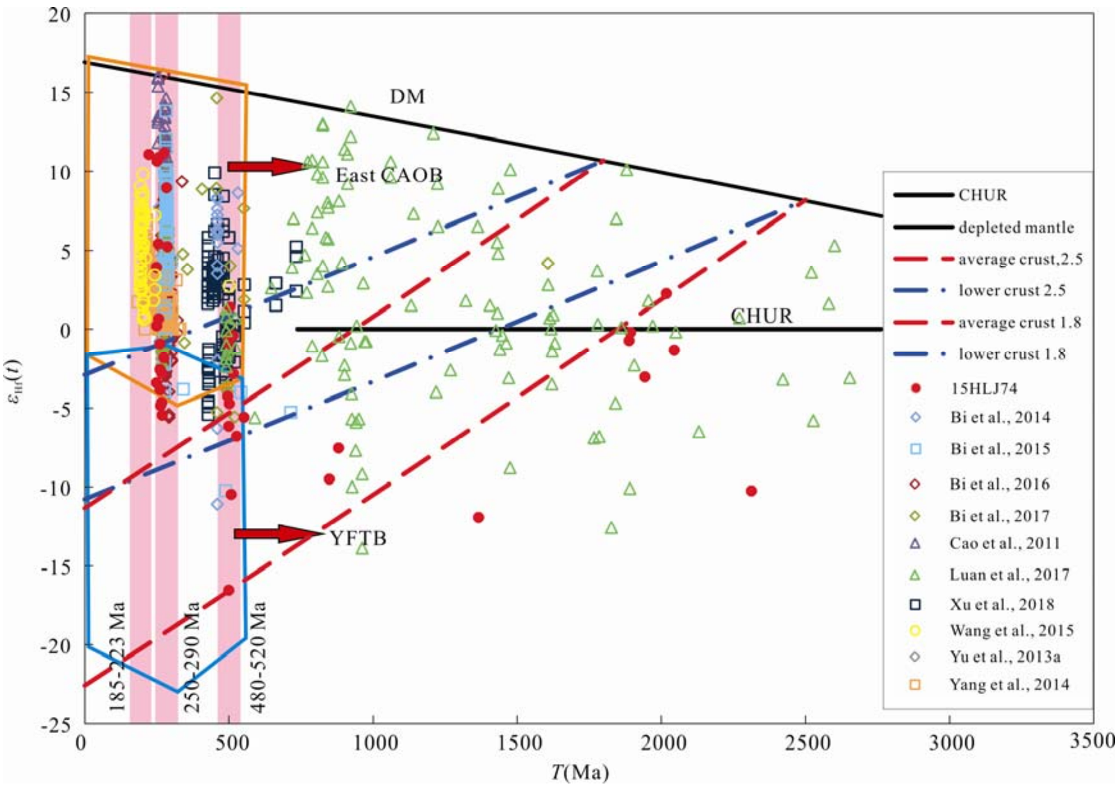

Fig. 8. Zircon $\varepsilon_{\rm Hf}(t)$ vs. T(Ma) diagram of intrusive and volcanic rocks of the Jiamusi-Khanka massif.
The zircon $\varepsilon_{\rm Hf}(t)$ were cited from Cao et al., 2011; Yu et al., 2013a; Bi et al., 2014, 2015, 2016, 2017; Yang et al., 2015; Luan et al., 2017; Xu et al., 2018. CAOB = Central Asian Orogenic Belt; YFTB = Yanshan Fold-and-Thrust Belt (Yang et al., 2006).

et al., 2017). The negative Hf isotope compositions of the zircons indicate that they were derived from magmas sourced from the reworking of ancient crust.

5 Disscusion on Sedimentary Provenance

The depositional age of Nanshuangyashan Formation was traditionally thought to be Late Triassic, according to rock associations and the Norian bivalve fauna (Zhou et al., 1962; HBGMR, 1993; Zhang et al., 2015). The present geochronological results provide reliable and tight constraints on the maximum depositional age of the Nanshuangyashan Formation, with the youngest zircon population at 223–215 Ma (peak at 218 Ma) (Figs. 7, 9) indicating that it was deposited after the Late Triassic. As shown in Figure 9, zircons age dating data show that the peak values of clastic zircons in the feldspar sandstones can be divided into four groups: 223–215 Ma, 287–244 Ma, 538–481 Ma and >800 Ma. The corresponding geological ages are Late Triassic, Middle Permian to Early Triassic, Cambrian and Precambrian respectively. Its sedimentary proenance is explained as follows.

5.1 Late Triassic magmatic events

Late Triassic ages of the detrial zircons from the Nanshuangyashan Formation range from 223 Ma to 215 Ma (Figs. 7, 9). Most zircon grains are euhedral shape with oscillation zones of igneous origin (Fig. 6). Similar ages were reported in the Jiamusi-Khanka massif near the Dunhua-Mishan Fault (Yang et al., 2015), Zhangguangcai Range on the eastern margin of the Songnen massif (Wu et al., 2002; Sun et al., 2005; Zhou et al., 2012; Wei, 2012; Wang et al., 2015), and southern Inner Mongolia (Li et al., 2013). Their $\varepsilon_{\rm Hf}(t)$ values of various areas are almost the same, and we cannot distinguish them. However, the maturity of debris particles is low, most of them are angular-subangular, poor sorting and calcareous cementation (Figs. 4c–f). Above all, we infer that the Nanshuangyashan Formation has a near-source characteristic. They were the result of deposition after the wreathing of nearby magmatic rocks.

5.2 Early Permian to Early Triassic magmatic events

Early Permian to Early Triassic ages of the detrial zircons from the Nanshuangyashan Formation range from 287 Ma to 244 Ma (Figs. 7, 9). Most zircon grains are euhedral shape with oscillation zones of igneous origin (Fig. 6). These age groups have been widely reported as magmatic events in the Jiamusi-Khanka and Songnen massif, including from gabbro, diorite, plagiogranite, granodiorite, monzogranite, graphic granite, alkali feldspar granite, and associated volcanic rocks, with zircon U-Pb ages from 296 Ma to 244 Ma (Wu et al., 2001, 2002; Huang et al., 2008; Wei, 2012; Yu et al., 2013a, 2013b; Bi et al., 2014, 2015, 2016, 2017; Pu et al., 2015; Sun et al., 2015; Dong et al., 2017b; Meng et al., 2008; Xu et al., 2012). In the Jiamusi-Khanka massif, these include the Liulian granodiorite (284±2 Ma) and hornblende-gabbro

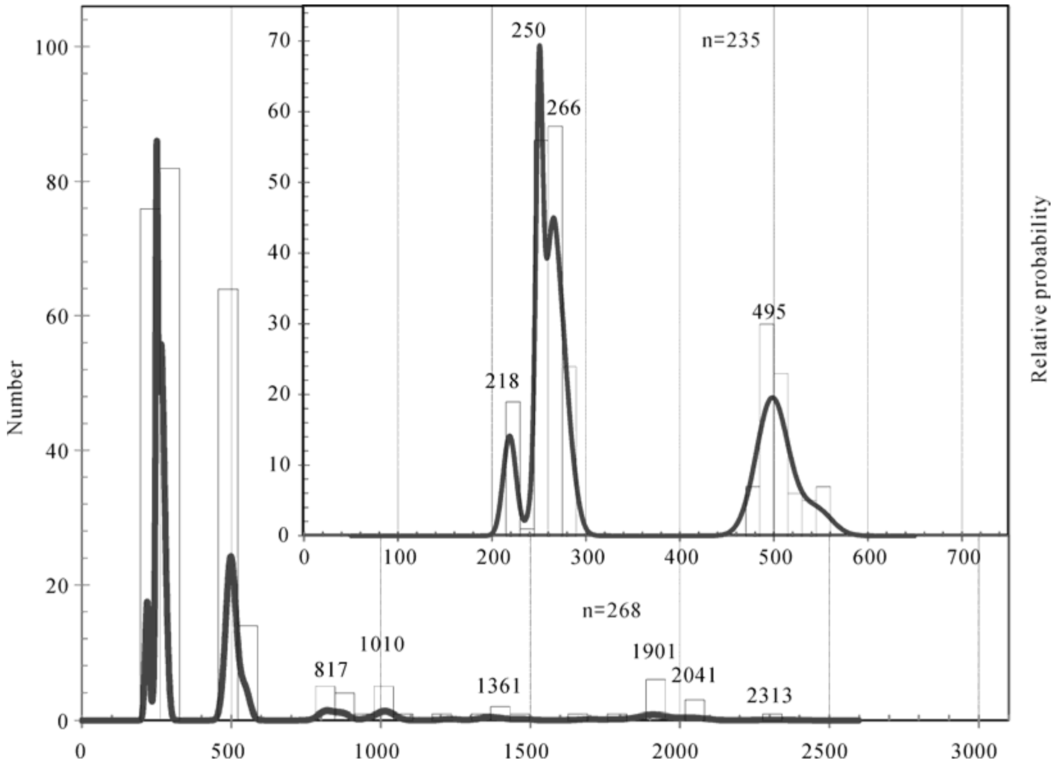

Fig. 9. Age histogram and relative probability diagram of detrital zircons from the Nanshuangyashan Formation.

(278±2 Ma) (Yu et al., 2013a), the Jinshan monzogranite (278-261 Ma) and granodiorite (260±8 Ma) (Bi et al., 2014), the Fangshan monzogranite (278-277 Ma) (Pu et al., 2015), the Shuguang gabbro (274±2 Ma) , plagiogranite (277±2 Ma), and the Rizhao gabbro (286–282 Ma) (Bi et al., 2015), the Liudao graphic granite (270±2 Ma), the Longtouqiao gabbro-diorite (275±2 Ma), the Liumao alkali feldspar granite (272±3 Ma), the Hongqi monzogranite (267±2 Ma), the Suolun monzogranite (282±2 Ma), the Tuanshan granodiorite (287±3 Ma), and the Yingchun granodiorite (293±2 Ma) (Bi et al., 2016), the Dongfanghong gabbro (276–274 Ma) (Sun et al., 2015), the Tiexi diorite (296±2 Ma), the Huafengshan monzogranite (295±3 Ma), the Chaoxiantun monzogranite (287±3 Ma), the Shuangyehu granite porphyry (258±2 Ma), and the Majiajie granodiorite (262±3 Ma) (Yang et al., 2015). In the Songnen-Zhangguangcai Range massif, these include the Fengmao monzogranite (262–261 Ma), the Dafenghe monzogranite (262±2 Ma), the Fenglin monzogranite (295±3 Ma), the Sandaolin monzogranite (260±1 Ma) and the Sihao granodiorite (244±2 Ma) (Wei, 2012), the Huangqigou monzogranite (256±1 Ma), the Xiaobeihu monzogranite (255±2 Ma) and the Lalagou granodiorite (252±2 Ma) (Yu et al., 2013b), the Mingyi granodiorite (278±2 Ma), the Tuoyaozi syengranite (276±3 Ma), the Mengjiagang monzogranite (272±5 Ma), the Hengtoushan monzogranite (267±3 Ma), and the Qinbei monzogranite (266–263 Ma) (Dong et al., 2017b). The ages of 296–244 Ma are also similar to the age of bimodal volcanics (293–263 Ma) from the Haojiatun, Dongshan, Zhenzishan, Erlongshan, Yanggang and Dalingqiao Formation (Meng et al., 2008; Bi et al., 2017). The detrital zircons are characterized by highly variable Lu-Hf isotopic compositions, with $\varepsilon_{\rm Hf}(t)$ values ranging from negative to positive within a single age group (Fig. 8). The ^{176}Hf/^{177}Hf ratios range from 0.282454 to 0.282921, corresponding to $\varepsilon_{\rm Hf}(t)$ values, Hf single-stage and two-stage model ages ($T_{\rm DM1}$ and $T_{\rm DM2}$) range from –11.2 to +10.9, from 1.12 to 0.46 Ga, and from 1.64 to 0.59 Ga, respectively (Table 3; Fig. 8). The $\varepsilon_{\rm Hf}(t)$ values ranging from negative to positive indicate that sedimentary provenance of the Nanshuangyashan Formation is a mixture result. Combined with published data (Cao et al., 2011; Wei, 2012; Yu et al., 2013a, 2013b; Bi et al., 2014, 2015, 2016, 2017; Yang et al., 2015; Ge et al., 2017), the $\varepsilon_{\rm Hf}(t)$ values of 287–249 Ma are consistent with these of the Jiamusi-Khanka and Songnen-Zhangguangcai Range massif. Therefore, the analysed zircons of 287–249 Ma, which were more likely derived from –259 Ma magmatic arcs, mostly have similar Hf isotopic compositions to those of zircons in the CAOB (Xiao et al., 2004 et al., Li et al., 2014, 2016, 2017;), but they differ from those of the Neoarchean and Paleoproterozoic zircons in the Paleozoic–Late Mesozoic strata of the Yanshan Fold and Thrust Belt (Yang et al., 2006).

5.3 Cambrian magmatic event and Late Pan-African event

We also obtained some Cambrian (538–481 Ma) zircons (Figs. 7, 9; Table 2). A likely provenance for these ages was identified, since some record of granulite facies metamorphic supracrustal rocks (–500 Ma) and granites (490–525 Ma) closely associated with them in the Jiamusi

-Khanka massif (Song et al., 1997; Wilde et al., 2000, 2001, 2003; Wu et al., 2001; Wen et al., 2008; Zhou et al., 2010; Zhang et al., 2012), which represents the final metamorphic consolidation age of the Precambrian Jiamusi-Khanka massif. And a time span of 25 Ma was recognized as late Pan-African in the Jiamusi massif (Wilde et al., 2003). In addition, similar ages were also reported in the Jiamusi-Khanka massif, with $\varepsilon_{Hf}(t)$ values ranging from negative to positive (Bi et al., 2014, 2017; Luan et al., 2017; Xu et al., 2018). The Cambrian detrial zircons from the Nanshuangyashan Formation show variable $\varepsilon_{Hf}(t)$ values (−16.5 to +1.4) (Fig. 8), indicating a mixed source from both juvenile crust and recycled older crust.

5.4 Implications of Precambrian zircon ages

Five very minor Precambrian zircon age groups of 881–805 Ma, 1042–960 Ma, 1391–1354 Ma, 1944–1889 Ma, and 2065–2018 Ma, with one zircon grain with an age of 2313 Ma, are present in the Nanshuangyashan Formation (Fig. 9). However, similar ages have not been reported from the basement rocks in the Jiamusi massif. A large number of studies have shown that the age groups of >800 Ma detrital or inherited zircons are ubiquitous in sedimentary and magmatic rocks of the Jiamusi massif (Li et al., 2013; Zhou et al., 2009a, 2010, 2011; Wilde et al., 2000; Luan et al., 2017), indicating that there is an older Precambrian continental crust in the Jiamusi massif. Also, the $\varepsilon_{Hf}(t)$ values of Precambrian zircon ages from the Nanshuangyashan Formation are similar to these from the Kimkanskaya Group and Majiajie Group (Luan et al., 2017) (Fig. 8), indicating a common source.

In summary, we suggest that the Nanshuangyashan Formation within the Jiamusi massif were sourced mainly from the Jiamusi-Khanka massif, and partly come from the Songnen-Zhangguangcai Range massif by the characteristics of rock structure, zircon ages, zircon Hf isotopes.

6 Tectonic Setting

Detrital zircon geochronology is rapidly evolving into a very powerful tool for determining the provenance and maximum depositional age of clastic strata. Large numbers of in situ, high precision analyses of both igneous and detrital zircons are now available, and a striking feature of the zircon record is that it clusters into peaks of crystallization ages (Condie et al., 2009). Hence, we focus the zircon ages and $\varepsilon_{Hf}(t)$ values of the Nanshuangyashan Formation to interpret tectonic evolution history of the Jiamusi massif. The eastern margin of the Jiamusi massif contains a set of Permian granites, with zircon ages between 294 and 258Ma (Wu et al., 2001, 2002; Huang et al., 2008; Yu et al., 2013a; Bi et al., 2014, 2015, 2016; Pu et al., 2015), and volcanic rocks, with zircon ages between 293 and 263 Ma (Meng et al., 2008; Bi et al., 2017). These granites and volcanic rocks are identified as magmatic arc origin on active continental margin by geochemical characteristics (Huang et al., 2008; Yu et al., 2013a; Bi et al., 2014, 2015, 2016, 2017). Also, Permian igneous rocks have also been recognized along the eastern margin of the Songnen-Zhangguangcai Range Massif, and like those of the Jiamusi Massif, these granitoids belong to the high-K calc-alkaline series, and are enriched in LREEs and LILEs and depleted in HREEs and HFSEs. Their geochemical characteristics are similar to volcanic arc granites, implying a subduction process during the formation of the granitoids (Dong et al., 2017b). In the western margin of the Jiamusi massif, the mafic intrusions (259–256Ma) and granitoids (–230 Ma), along the boundary area of the Jiamusi massif and Songnei-Zhangguangcai Rang massif, provides further evidence for the eastward subduction of the Mudanjiang ocean (Wei, 2012; Dong et al. 2017a).As noted above, the geochronological results and $\varepsilon_{Hf}(t)$ values of the Nanshuangyashan Formation can provide the maximum age of deposition and sedimentary provenance. However, when combined with the fossil evidence, they suggest that the deposition age of the Nanshuangyashan Formation was between 227 Ma and 218 Ma. Yang et al. (1998) reported that the Yuejinshan Complex undergone greenschist-facies metamorphism with a deformation at 188 Ma. In addition, high-pressure metamorphic blueschist is widely exposed in the Heilongjiang HP Belt along the western margin of the Jiamusi-Khanka massif. Zhou (2009) reported that magmatic zircons from two samples of epidote-blueschist facies metabasalts from the Heilongjiang HP belt have SHRIMP U-Pb $^{206}Pb/^{238}U$ ages of 213 Ma and 224 Ma, whereas the biotite Rb-Sr mineral isochron age of 184±4 Ma from a dioritic gneiss from Luobei, and mica schist from Yilan gave phengite $^{40}Ar/^{39}Ar$ ages of 175–173 Ma (Wu et al., 2007). Namely, the metamorphism of the Heilongjiang HP Belt took place between 210 and 180 Ma, and was related to the onset of Paleo-Pacific plate subduction (Zhou et al., 2009b, 2014; Zhou and Wilde, 2013). Therefore, we propose a cartoon sketch of the proposed tectonic setting from Late Carboniferous to Early Jurassic in the eastern of Jiamusi massif is as follows.

(1) During Late Carboniferous to Late Permian (305–260 Ma), the eastern margin of Jiamusi massif formed continental arc and accretionary prim caused by the oceanic plate (Fig. 10a). Owing to the subduction of oceanic plate, the Longtouqiao gabbro–diorites in the eastern margin of Jiamusi massif coexisted closely with the granitoids in space and time, and together they exhibit a bimodal signature typical of extensional settings. The geochemical characters indicate that the eastern margin of Jiamusi massif appear to be a subduction zone or an arc affinity. The combined occurrence of 272 Ma A-type Liumao granites in the Baoqing area, 290–274 Ma gabbros in the Dongfanghong area (Bi et al., 2015; Sun et al., 2015), 284–278 Ma magma mixing in the Liulian area (Yu et al., 2013), and the coeval volcano (Meng et al. 2008; Bi et al., 2017) indicates that Permian intrusive rocks were emplaced in an extensional setting, and that they represent a transitional change from compression to extension in the geodynamic regime. At the same time new oceanic crust was generated and collaged into the eastern margin of Jiamusi massif. While, in the western margin of the Jiamusi massif, a Permian (278–260 Ma) N-S trending granitoid belt was formed by the eastwards subduction of the Mudanjiang ocean (Wei, 2012; Dong et al., 2017b).

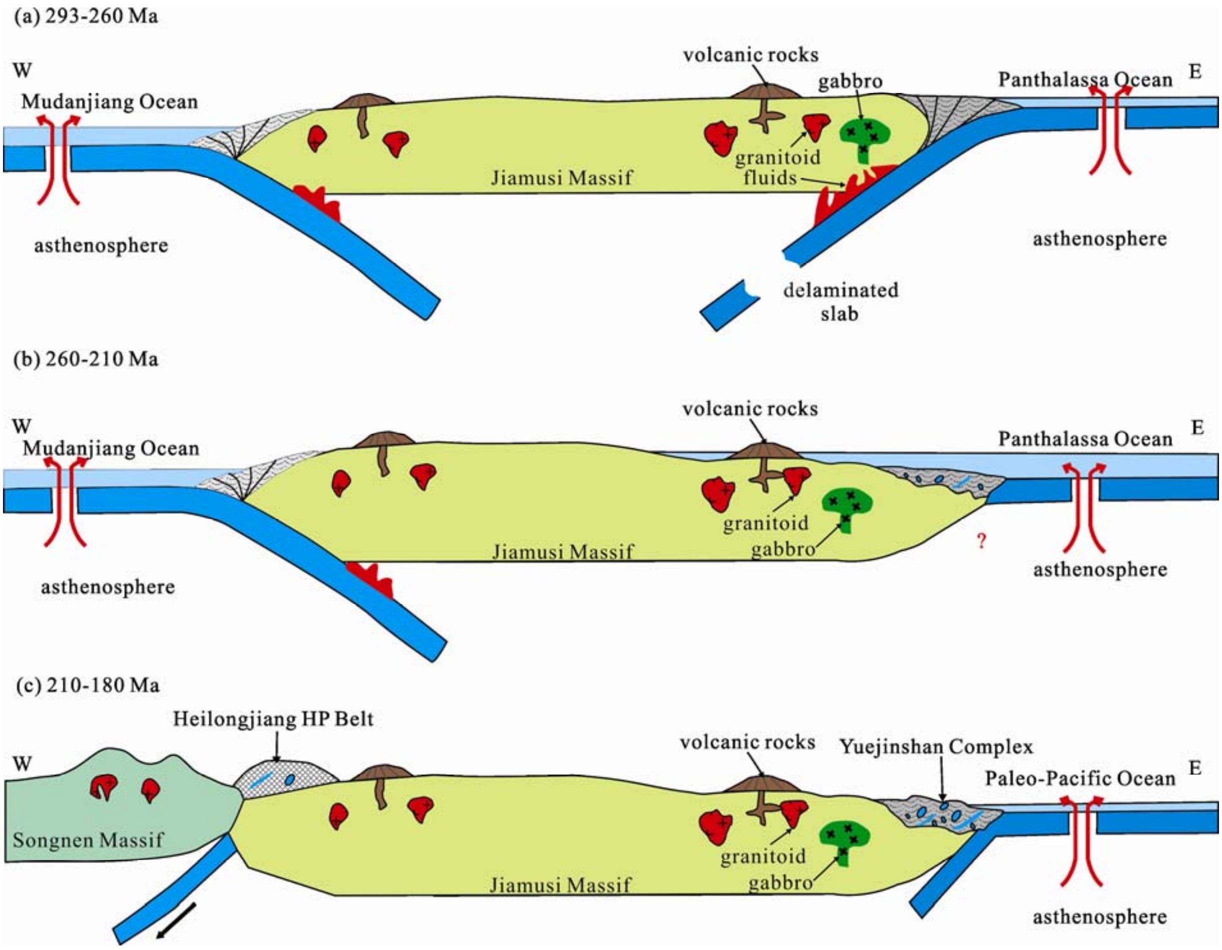

Fig. 10. A cartoon sketches of the proposed tectonic setting of the transform in the eastern of Jiamusi massif.

(2) From Late Permian to Late Triassic (260–210 Ma), continental crust subsidence occurred during transgression in the eastern margin of Jiamusi massif (Fig. 10b). There developed a suite marine-land interbedded stratum, called Nanshuangyashan Formation, along passive continental margin in the eastern margin of the Jiamusi massif. In the western margin of the Jiamusi massif, the mafic intrusions (259–256Ma) and granitoids (–230 Ma), along the boundary area of the Jiamusi massif and Songnei-Zhangguangcai Rang massif, provides further evidence for the eastward subduction of the Mudanjiang ocean (Wei, 2012; Dong et al. 2017a).

(3) From Late Triassic to Early Jurassic (210–180 Ma), westward obduction of the Paleo-Pacific plate over the Jiamusi massif resulted in the emplacement of the Yuejinshan Complex (Fig. 10c). Also, the Heilongjiang HP Belt was formed by the Paleo-Pacific subduction (Zhou et al., 2009b, 2014).

7 Conclusions

Based on the U-Pb zircon ages and Hf isotopic data presented in this paper, we draw the following conclusions.

(1) U-Pb detrital zircon dating of the Nanshuangyashan Formation defines the youngest age cluster at –218 Ma, indicating the maximum depositional age. Namely, the Nanshuangyashan Formation, which is unconformable over the Permian granites in the eastern margin of the Jiamusi massif, was depositing in the Late Triassic.

(2) The Nanshuangyashan Formation within the Jiamusi massif were sourced mainly from the Jiamusi-Khanka massif, and partly come from the Zhangguangcai Early Mesozoic granites in the eastern margin of the Songnen massif.

Acknowledgements

We are grateful to Yang Yueheng and Ma Qian of the Institute of Geology and Geophysics, Chinese Academy of Sciences (Beijing), China, for their advice and assistance during Lu-Hf isotope analyses. We thank the Key Laboratory of Mineral Resources Evaluation in Northeast Asia, Ministry of Land and Resources, Jilin University, Changchun, China for assistance in zircon U-Pb dating. The final version of this paper benefited from perceptive comments by Li Shan (Guest Editor) and two anonymous reviewers. This study is financially supported by National Natural Science Foundation of China (Grant No. 41474081) and the projects from China Geological Survey

(Grant No. 1212011120973).

Manuscript received May 15, 2019
accepted Aug. 14, 2019
associate EIC XIAO Wenjiao
edited by LIU Lian

References

Belousova, E., Griffin, W., O'Reilly, S.Y. and Fisher, N., 2002. Igneous zircon: trace element composition as an indicator of source rock type. Contributions to Mineralogy and Petrology, 143(5): 602–622.

Bi, J.H., Ge, W.C., Yang, H., Wang, Z.H., Dong, Y., Liu, X.W. and Ji, Z., 2017. Age, petrogenesis, and tectonic setting of the Permian bimodal volcanic rocks in the eastern Jiamusi Massif, NE China. Journal of Asian Earth Sciences, 134: 160–175.

Bi, J.H., Ge, W.C., Yang, H., Wang, Z.H., Xu, W.L., Yang, J.H., Xing, D.H. and Chen, H.J., 2016. Geochronology and geochemistry of late Carboniferous–middle Permian I- and A-type granites and gabbro–diorites in the eastern Jiamusi Massif, NE China: Implications for petrogenesis and tectonic setting. Lithos, 266–267: 213–232.

Bi, J.H., Ge, W.C., Yang, H., Zhao, G.C., Xu, W.L. and Wang, Z.H., 2015. Geochronology, geochemistry and zircon Hf isotopes of the Dongfanghong gabbroic complex at the eastern margin of the Jiamusi Massif, NE China: Petrogensis and tectonic implications. Lithos, 234–235: 27–46.

Bi, J.H., Ge, W., Zhang, Y.L., Yang, H. and Wang, Z.H., 2014. Petrogenesis of Permian Jinshan Granitic Complex in the Eastern Jiamusi Massif and Its Geological Implications. Journal of Earth Sciences & Environment, 36(4): 16–31 (in Chinese with English abstract).

Buslov, M.M., Fujiwara, Y., Iwata, K. and Semakov, N.N., 2004. Late Paleozoic-Early Mesozoic Geodynamics of Central Asia. Gondwana Research, 7(3): 791–808.

Bussien, D., Gombojav, N., Winkler, W. and von Quadt, A., 2011. The Mongol–Okhotsk Belt in Mongolia—An appraisal of the geodynamic development by the study of sandstone provenance and detrital zircons. Tectonophysics, 510(1–2): 132–150.

Cao H.H., Xu W.L., Pei F.P., Zhang X.Z., 2011. Permian tectonic evolution in southwestern khanka massif:evidence from zircon U-Pb chronology, Hf isotope and geochemistry of gabbro and diorite. Acta Geologica Sinica (English Edition), 85(6): 1390–1402.

Condie, K.C., Belousova, E., Griffi n, W.L., and Sircombe, K.N., 2009. Granitoid events in space and time: Constraints from igneous and detrital zircon age spectra. Gondwana Research, 15(3–4): 228–242.

Dobretsov, N., Buslov, M. and Zhimulev, F., 2005. Cambrian-Ordovician tectonic evolution of the Kokchetav metamorphic belt, northern Kazakhstan. Russian Geology and Geophysics, 46(8): 785–795.

Dong, Y., Ge, W.C., Yang, H., Bi, J.H., Wang, Z.H., Xu, W.L., 2017a. Permian tectonic evolution of the Mudanjiang Ocean: Evidence from zircon U-Pb-Hf isotopes and geochemistry of a N-S trending granitoid belt in the Jiamusi Massif, NE China. Gondwana Research, 49: 147–163.

Dong, Y., Ge, W.C., Yang, H., Xu, W.L., Bi, J.H., Wang, Z.H., 2017b. Geochemistry and geochronology of the Late Permian mafic intrusions along the boundary area of Jiamusi and Songnen-Zhangguangcai Range massifs and adjacent regions, northeastern China: Petrogenesis and implications for the tectonic evolution of the Mudanjiang Ocean. Tectonophysics, 694: 356–367.

Eggins, S.M., Kinsley, L.P.J., and Shelley, J.M.M., 1998. Deposition elemental fractionation processes during atmospheric pressure laser sampling for analysis by ICP–MS. Applied Surface Science, 127–129: 278–286.

Fu, Q.L., ZHANG, X.Z., ZENG, Z. and Pu J.B., 2016. Discovery and tectonic significance of unconformity in Devonian with its underlying metamorphic basement in Fujin uplift. Global Geology, 35(2): 458–469 (in Chinese with English abstract).

Ge, M.H., Zhang, J.J., Li, L., Liu, K., Ling, Y.Y., Wang, J.M., Wang M., 2017. Geochronology and geochemistry of the Heilongjiang Complex and the granitoids from the Lesser Xing'an-Zhangguangcai Range: implications for the late Paleozoic-Mesozoic tectonics of eastern NE China. Tectonophysics, 717: 565–584.

Ge, W.C., Wu, F.Y., Zhou, C.Y., and Rahman, A.A., 2005. Emplacement age of the Tahe granite and its constraints on the tectonic nature of the Ergun block in the northern part of the Da Hinggan Range. Chinese Science Bulletin, 50(18): 2097–2105.

Griffin, W.L., Pearson, N.J., Belousova, E., Jackson, S.E., Achterbergh, E., Reilly, S.Y., Shee, S.R., 2000. The Hf isotope composition of cratonic mantle: LAM–MC–ICPMS analysis of zircon megacrysts in kimberlites. Geochimica et Cosmochimica Acta, 64(1): 133–147.

Heilongjiang Bureau of Geology and Mineral Resources (HBGMR) 1987. 1:200000 Regional geological Map of Xaojiahe and Raohe. Beijing: Geol. Publ. House (in Chinese).

Heilongjiang Bureau of Geology and Mineral Resources (HBGMR) 1993. Regional geology of Heilongjiang Province. Beijing: Geol. Publ. House (in Chinese with English abstract).

Huang, B.H., 1982. The Carboniferous–Permian terrestrial strata in the north part of the northeastern China. Geological Review, 28(5): 395–401 (in Chinese).

Huang, T.K., Jen, C.S., Jiang, C.F., Zhang, Z.M., and Xu, Z.Q., 1997. An outline of the tectonic characteristics of China. Earth Science, 36(5): 288–303.

Huang, Y.C., Ren, D.H., Zhang, X.Z., Xiong, X.S., Zhang, C.Y., Wang, Y., and Zhao, L.L., 2008. Zircon U–Pb dating of the Meizuo granite and geological significance in the Huanan uplift, east Heilongjiang Province. Journal of Jilin University (Earth Science Edition), 38(4): 631–638 (in Chinese with English abstract).

Jackson, S.E., Pearson, N.J., Griffin, W.L., and Belousova, E.A., 2004. The application of laser ablation–inductively coupled plasma–mass spectrometry to in situ U–Pb zircon geochronology. Chemical Geology, 211(1–2): 47–69.

Kang BX. 1979. Stratigraphic table of Heilongjiang Province. Harbin: Heilongjiang Publishing House (in Chinese).

Karsakov, L.P., Zhao, C.H., Goroshko, M.V., Roganov, G.V., Varnavsky, V.G., Mishin, L.F., Malyshev, Y.F., Lu, Z., Gornov, P.Y., and Kaplun, V.B., 2005. Tectonics, deep structure, metallogeny of the Central Asian–Pacific belts junction area: Explanatory Notes to the Tectonic Map Scale of, 1 (1,500,000).

Khanchuk, A.I., 2001. Pre-Neogene tectonics of the Sea-of-Japan region: A view from the Russian side (< Special issue> Geotectonic framework of eastern Asia before the opening of the Japan Sea-Part 2-). Earth Science (Chikyu Kagaku), 55(5): 275–291.

Koschek, G., 1993. Origin and significance of the SEM cathodoluminescence from zircon. Journal of Microscopy, 171: 223–232.

Li, J.Y., 1998. Some new ideas on tectonics of NE China and its neighboring areas. Geological Review, 44(4): 339–347 (in Chinese with English abstract).

Li, S., Wang, T., Wilde S.A., and Tong Y., 2013. Evolution, source and tectonic significance of Early Mesozoic granitoid magmatism in the Central Asian Orogenic Belt (central segment). Earth-Science Reviews, 126: 206–234.

Li, S., Chung, S.L., Wilde, S.A., Wang, T., Xiao, W.J., and Guo, Q.Q., 2016. Linking magmatism with collision in an accretionary orogen. Scientific Reports, 6(1): 25751.

Li, S., Wilde, S.A., He, Z., Jiang, X., Liu, R., and Zhao, L., 2014. Triassic sedimentation and postaccretionary crustal evolution along the solonker suture zone in Inner Mongolia, China. Tectonics, 33(6): 960–981.

Li, S., Chung, S.L., Wilde, S.A., Jahn, B.M., Xiao, W.J., Wang, T., and Guo, Q.Q., 2017. Early-Middle Triassic high Sr/Y granitoids in the southern Central Asian Orogenic Belt: Implications for ocean closure in accretionary orogens. Journal of Geophysical Research: Solid Earth, 122(6): 2291–2309

Luan J.P., Wang F., Xu W.L., Ge W.C., Sorokin A.A., Wang Z.H.,

Guo P., 2017. Provenance, age, and tectonic implications of Neoproterozoic strata in the Jiamusi Massif: evidence from U–Pb ages and Hf isotope compositions of detrital and magmatic zircons. Precambrian Research. 297: 19–32.
Ludwig, K.R., 2003. Isoplot 3.09-A geochronological toolkit for Microsoft Excel. Berkeley Geochronology Center Special Publication, 1–4.
Machado, N., Simonetti, A., 2001. U–Pb dating and Hf isotopic composition of zircons by laser ablation–MC–ICP–MS. In: Sylvester, P. (Ed.), Laser Ablation ICPMS in the Earth Sciences: Principles and Applications. Short Course, Mineralogical Association of Canada, 29: 121–146.
Meng, E., Xu, W.L., Yang, D.B., Pei, F.P., Yu, Y., and Zhang, X.Z., 2008. Permian volcanisms in eastern and southeastern margins of the Jiamusi Massif, northeastern China: zircon U-Pb chronology, geochemistry and its tectonic implications. Chinese Science Bulletin, 53(8): 1231–1245.
Pu, J.B., Zhang, X.Z., Guo Y., Zeng Z., Fu Q.L., Zhang H.T., Liu Y., 2015. Geological implications of Permian Fangshan granitic rocks in eastern Jiamusi Massif: evidences from U-Pb chronology and geochemistry. Global Geology, 34(4): 903–913 (in Chinese with English abstract).
Qu G.S., 1997. Lithostratigraphy of Heilongjiang Province. Wu Han: China University of Geosciences Press.1–298 (in Chinese).
Sengör, A.M.C., and Natal'in, B.A., 1996. Paleotectonics of Asia: fragments of a synthesis. In: Yin, A., Harrison, T.M. (Eds.), The Tectonics of Asia. Cambridge University Press, New York, 486–640.
Sláma, J., Kosler, J., Condon, D.J., Crowley, J.L., Gerdes, A., Hanchar, J.M., Horstwood, M.S.A., Morris, G.A., Nasdala, L., Norberg, N., Schaltegger, U., Schoene, B., Tubrett, M.N., Whitehouse, M.J., 2008. Plešovice zircon — a new natural reference material for U–Pb and Hf isotopic microanalysis. Chemical Geology (1–2), 249: 1–35.
Song, B., Li, J.Y., and Niu B.G., 1997. Single-Grain Zircon Ages and Its Implications in Biotite-Plagioclase Gneiss in Mashan Group in the Eastern Heilongjiang. Act Geoscientica Sincia, 18(3): 306–312 (in Chinese with English abstract).
Sorokin, A.A., Kolesnikov, A.A., Kotov, A.B., and Kovach, V.P., 2014. Areas and sources of Paleozoic metaterrigenous rocks of the Yankan terrane in the Mongolia-Okhotsk foldbelt: Evidence from the Sm-Nd isotope-geochemical studies. Doklady Earth Sciences. 545(2): 204–207.
Sun, D.Y., Wu, F.Y., Gao, S. and Lu, X.P., 2005. Confirmation of two episodes of A-type granite emplacement during Late Triassic and Early Jurassic in the central Jilin Province, and their constraints on the structural pattern of Eastern Jilin–Heilongjiang Area. China. Earth Science Frontiers 12(2): 263–275.
Sun, M.D., Xu, Y.G., Wilde, S.A., Chen, H.L., and Yang, S.F., 2015. The Permian Dongfanghong island-arc gabbro of the Wandashan Orogen, NE China: Implications for Paleo-Pacific subduction. Tectonophysics, 659: 122–136.
Wang, C.W., Jin, W., Zhang, X.Z., Ma, Z.H., Chi, X.G., Liu, Y.Y., and Li, N., 2008. New understanding of the Late Paleozoic tectonics in northeastern China and adjacent areas. Journal of Stratigraphy, 32(2): 119–136 (in Chinese with English abstract).
Wang, F., Xu, W.L., Xu, Y.G., Gao, F.H., and Ge, W.C., 2015. Late Triassic bimodal igneous rocks in eastern Heilongjiang Province, NE China: Implications for the initiation of subduction of the Paleo-Pacific Plate beneath Eurasia. Journal of Asian Earth Sciences, 97: 406–423.
Wei, H.Y., 2012. Geochronology and petrogenesis of granitoids in Yichun-Hegang, Area, Heilongjiang Province. (Ph.D. thesis). Jilin University,1–66 (in Chinese with English abstract)
Wen, Q.B., Liu, Y.J., Li, W.M., Han, G.Q., and Ding, L., 2008. Monazite age and its geological significance of granitoid gneiss in the Jiamusi Massif. Journal of Jilin University (Earth Science Edition), 38(2): 187–193 (in Chinese with English abstract).
Wiedenbeck, M., Alle, P., Corfu, F., Griffin, W.L., Meier, M., Oberli, F., Quadt, A., Roddick, J.C., and Spiegel, W., 1995. Three natural zircon standards for U-Th-Pb, Lu-Hf, trace element and REE analyses. Geostandards Newsletter, 19: 1–23.
Wilde, S.A., Wu, F.Y., and Zhang, X.Z, 2001. The Mashan Complex: SHRIMP U–Pb zircon evidence for a Late Pan-African metamorphic event in NE China and its implication for global continental reconstructions. Geochimica, 30(1): 35–50 (in Chinese with English abstract).
Wilde, S.A., Wu, F.Y., and Zhang, X.Z., 2003. Late Pan-African magmatism in northeastern China: SHRIMP U–Pb zircon evidence from granitoids in the Jiamusi Massif. Precambrian Research, 122(1–4): 311–327.
Wilde, S.A., Zhang, X.Z., and Wu, F.Y., 2000. Extension of a newly identified 500Ma metamorphic terrane in North East China: further U–Pb SHRIMP dating of the Mashan Complex, Heilongjiang Province, China. Tectonophysics, 328(1–2): 115–130.
Wu, F.Y., Jahn, B.M., Wilde, S.A., Lo, C.H., Yui, T. F., Lin, Q., Ge, W.C., and Sun, D.Y., 2003. Highly fractionated I-type granites in NE China (I): geochronology and petrogenesis. Lithos, 66(3–4): 241–273.
Wu, F.Y., Li, X.H., Zheng, Y.F., Gao, S., 2007. Lu–Hf isotopic systematics and their applications in petrology. Acta Petrologica Sinica, 23(2): 185–220 (in Chinese with English abstract).
Wu, F.Y., Sun, D.Y., Li, H.M., Jahn, B.M., and Wilde, S.A., 2002. A-type granites in northeastern China: age and geochemical constraints on their petrogenesis. Chemical Geology, 187(1–2): 143–173.
Wu, F.Y., and Sun, D.Y., 2001. Zircon SHRIMP U-Pb ages of gneissic granites in Jiamusi massif. Acta Petrologica Sinica, 17(3): 443–452 (in Chinese with English abstract).
Wu, Y.B., and Zheng, Y.F., 2004. Genesis of zircon and its constraints on interpretation of U-Pb age. Chinese Science Bulletin, 49(15): 1554–1569.
Wu, F.Y., Yang J.H., Lo C.H., Wilde S.A., Sun D.Y., and Jahn B.M., 2007. The Heilongjiang Group: A Jurassic accretionary complex in the Jiamusi Massif at the western Pacific margin of northeastern China. Island Arc, 16(1): 156–172.
Wu, F.Y., Yang, Y.H., Xie, L.W., Yang, J.H., Xu, P., 2006. Hf isotopic compositions of the standard zircons and baddeleyites used in U–Pb geochronology. Chemical Geology, 234(1–2): 105–126.
Xiao,W.J., Zhang, L.C., Qin, K.Z., Sun, S., Li, J.Y., 2004. Paleozoic accretionary and collisional tectonics of the eastern Tienshan (China): implications for the continental growth of Central Asia. American Journal of Science, 304(4): 370–395.
Xu, T., Xu, W.L., Wang, F., Ge, W.C., Sorokin, A.A., 2018. Geochronology and Geochemistry of Early Paleozoic Intrusive Rocks from the Khanka Massif in the Russian far East: Petrogenesis and Tectonic Implications. Lithos, 300–301: 105–120.
Xu, P., Wu, F.Y., Xie, L.W., Yang, Y.H., 2004. Hf isotopic compositions of the standard zircons for U–Pb dating. Science Bulletin, 49(15): 1642–1648.
Xu, W.L., Wang, F., Meng, E., Gao, F.H., Pei, F.P., Yu, J.J., and Tang, J., 2012. Paleozoic-Early Mesozoic tectonic evolution in the eastern Heilongjiang Province, NE China: Evidence from igneous rock association and U-Pb geochronology of detrital zircons. Journal of Jilin University (Earth Science Edition), 42 (5): 1378–1389 (in Chinese with English abstract).
Yang, H., Ge, W.C, Zhao, G.C., Yu, J.J., and Zhang, Y.L., 2015. Early Permian–Late Triassic granitic magmatism in the Jiamusi–Khanka Massif, eastern segment of the Central Asian Orogenic Belt and its implications. Gondwana Research, 27 (4): 1509–1533.
Yang, J.Z., Qiu, H.J., Sun, J.P., Zhang, X.Z., 1998. Yuejinshan Complex and its tectonic significance. Journal of Changchun University of Science and Technology, 28(4): 380–385 (in Chinese with English abstract).
Yu, J.J., Hou, X.G., Ge, W.C., Zhang, Y.L., and Liu, J.C., 2013a. Magma mixing genesis of the Early Permian Liulian pluton at the northeastern margin of the Jiamusi massif in NE China: evidences from petrography, geochronology and geochemistry. Acta Petrologica Sinica, 29(9): 2971–2986 (in

Chinese with English abstract).
Yu, J.J., Wang, F., Xu, W.L., Gao, F.H., Tang, J., 2013b. Late Permian tectonic evolution at the southeastern margin of the Songnen-Zhangguangcai Range Massif, NE China: Constraints from geochronology and geochemistry of granitoids. Gondwana Research, 24 (2): 635–647.
Yuan H.L., Gao S., Liu X.M., Li H.M., Günther D. and Wu F.Y., 2004. Accurate U-Pb age and trace element determinations of zircon by laser ablation-inductively coupled plasma-mass spectrometry. Geostandards and Geoanalytical Research, 28(3): 353–370.
Zhang, X.Z., Ma, Y.X., Chi, X.G., Zhang, F.X., Sun, Y.W., Guo, Y., and Zeng, Z., 2012. Discussion on Phanerozoic tectonic evolution in Northeastern China. Journal of Jilin University (Earth Science Edition), 42(5): 1269–1285 (in Chinese with English abstract).
Zhang, X.Z, Qiao, D.W., Chi, X.G., Zhou, J.B., Sun, Y.W., Zhang, F.X., Zhang, S.Q., and Zhao, Q.Y, 2011. Late-Paleozoic tectonic evolution and oil-gas potentiality in northeastern China. Geological Bulletin of China, 30(2): 205–213 (in Chinese with English abstract).
Zhang, X.Z, Zhou, J.B., Chi, X.G., Wang, C.W., and Hu, D.Q., 2008. Late Paleozoic tectonic-sedimentation and petroleum resources in northeastern China. Journal of Jilin University (Earth Science Edition), 38(5): 719–725 (in Chinese with English abstract).
Zhang, X.Z., Guo, Y., Zhou, J.B., Zeng, Z., Pu, J.B., and Fu, Q.L., 2015. Late Paleozoic-Early Mesozoic tectonic evolution in the east margin of the Jiamusi massif, eastern northeastern China. Russian Journal of Pacific Geology, 9(1): 1–10.
Zhou, J.B., Cao, J.L., Wilde, S.A., Zhao, G.C., Zhang, J.J., and Wang, B., 2014. Paleo‐Pacific subduction-accretion: Evidence from Geochemical and U‐Pb zircon dating of the Nadanhada accretionary complex, NE China. Tectonics, 33: 2444–2466.
Zhou, J.B., and Wilde S A., 2013. The crustal accretion history and tectonic evolution of the NE China segment of the Central Asian Orogenic Belt. Gondwana Research, 23(4): 1365–1377.
Zhou, J.B., Wilde, S.A., Zhang, X.Z., Zhao, G.C., Liu, F.L., Qiao, D.W., Ren, S.M., and Liu, J.H., 2011a. A >1300 km late Pan-African metamorphic belt in NE China: New evidence from the Xing'an block and its tectonic implications. Tectonophysics, 509(3–4): 280–292.
Zhou, J.B., Wilde, S.A., Zhao, G.C., Zhang, X.Z., Zheng, C.Q., Wang, H.U., and Zeng, W.S., 2010. Pan-African metamorphic and magmatic rocks of the Khanka Massif, NE China: further evidence regarding their affinity. Geological Magazine, 147 (5): 737–749.
Zhou, J.B., Zhang, X.Z., and Ma, Z.H., Liu, L., Jin, W., Zhang, M.S., Wang, C.W., Chi, X.G., 2009a. Tectonic framework and basin evolution in Northeast China. Oil & Gas Geology, 30 (5): 530–538 (in Chinese with English abstract).
Zhou, J. B., Wilde, S. A., Zhang, X. Z., Zhao, G. C., Zheng, C. Q., Wang, Y. J., Zhang, X. H., 2009b. The onset of Pacific margin accretion in NE China: Evidence from the Heilongjiang high‐pressure metamorphic belt. Tectonophysics, 478(3–4): 230–246.
Zhou, J.B., Zhang, X.Z., Wilde, S.A., and Zheng, C., 2011b. Confirming of the Heilongjiang ~500 Ma Pan-African khondalite belt and its tectonic implications. Acta Petrologica Sinica, 27(4): 1235–1245 (in Chinese with English abstract).
Zhou Q.R., 1962. Regional geological survey report of Baoqing. Harbin: Heilongjiang Publishing House (in Chinese).

About the first author

CUI Weilong, Male, born in 1993 in Qiqihaer City; PhD in Institute of Geology and Geophysics, Chinese Academy of Sciences; Major in petrology. Email: geo_cuiwl@126.com; phone: 16601049044

About the corresponding author

ZENG Zhen, male, born in 1989 in Tonghua City, Jilin Province; doctor; graduated from Jilin University; Engineer of Institute of Geomechanics, Aerospace Architectural Design and Research Institute. Email: 23911989@qq.com; phone: 010-89060836.